

# Effect of topographic slope on the export of nitrate in humid catchments: a 3D model study

Jie Yang<sup>1</sup>, Qiaoyu Wang<sup>1</sup>, Ingo Heidbüchel<sup>2, 4</sup>, Chunhui Lu<sup>1</sup>, Yueqing Xie<sup>3</sup>, Andreas Musolff<sup>2</sup>, and Jan H. Fleckenstein<sup>2, 4</sup>

<sup>1</sup>State Key Laboratory of Hydrology-Water Resources and Hydraulic Engineering, Hohai University, Nanjing, China

<sup>2</sup>UFZ - Helmholtz-Centre for Environmental Research GmbH, Department of Hydrogeology, Leipzig, Germany

<sup>3</sup>School of Earth Sciences and Engineering, University of Nanjing, Nanjing, China

<sup>4</sup>Hydrologic Modeling Unit, Bayreuth Center of Ecology and Environmental Research (BayCEER), University of Bayreuth, Bayreuth, Germany

Correspondence to: Jie Yang ([yangj@hhu.edu.cn](mailto:yangj@hhu.edu.cn)); Chunhui Lu ([clu@hhu.edu.cn](mailto:clu@hhu.edu.cn))

## Key Points

- Young water fractions of Q and ET are correlated to topographic slope negatively and positively, respectively affects in-stream nitrate concentrations in a three-class pattern rather than being exclusively monotonous
- Young streamflow fraction and nitrate concentration decrease sharply once flatter landscapes are not able to maintain fast preferential overland flow paths. Flatter landscapes tend to retain more nitrogen mass in the soil and export less nitrogen mass to the stream
- High level of a large young streamflow fractions is not sufficient for high level of in-stream nitrate concentrations. The seasonal fluctuation of in-stream concentration is caused mainly by the temporal variability of nitrate degradation for catchments in temperate humid climates
- Seasonal fluctuations tend to be more pronounced in flatter landscapes.

**Abstract.** Excess export of nitrate to streams affects ecosystem structure and functions and has been an environmental issue attracting world-wide attention. The dynamics of catchment-scale solute export from diffuse nitrate-nitrogen sources can be explained by the activation and deactivation changes of dominant flow paths, as solute attenuation (including the degradation of nitrate) is linked to the age composition of outflow. Previous data driven studies suggested that catchment topographic slope has strong impacts on the age composition of streamflow and consequently on in-stream solute concentrations. However, the impacts have not been systematically assessed in terms of solute mass fluxes and solute concentration levels and variation, particularly in humid catchments with strong

34 seasonality in meteorological forcing. To fill this gap, we modeled the groundwater flow and nitrate transport for a  
35 ~~cross-section of~~ a small agricultural catchment in Central Germany. We used the fully coupled surface and subsurface  
36 numerical simulator HydroGeoSphere (HGS) to model groundwater and overland flow as well as nitrate  
37 ~~transporte~~ concentrations. We computed the water ages using numerical tracer experiments. To represent various  
38 topographic slopes, we additionally simulated ten synthetic ~~cross-sections~~ catchments generated by modifying the  
39 ~~topographic mean~~-slope from the real-world scenario ~~while preserving the land surface micro-topography~~. Results  
40 suggest a ~~negative correlation~~ ~~three-class response of~~ between ~~the young streamflow fraction and in-stream nitrate~~  
41 ~~concentrations to~~ the topographic slope. ~~This correlation is more pronounced in the flat landscapes with slopes <~~  
42 ~~1:60 from class 1 (slope > 1:60), via class 2 (1:100 < slope < 1:60), to class 3 (slope < 1:100). Flatter landscapes tend~~  
43 ~~to retain more N mass in the soil (including mass degraded in soil) and export less N mass to the stream, due to the~~  
44 ~~reduced leaching- and improved degradation in flatter landscapes. The mean in-stream nitrate concentration~~  
45 ~~shows a decreasing trend in response to the decreasing topographic slope, suggesting that a large high level of young~~  
46 ~~streamflow fractions is not sufficient for a high level of in-stream concentrations. Flatter landscapes tend to produce~~  
47 ~~higher in-stream nitrate concentrations within class 1 or class 3, however, not within class 2. Young streamflow~~  
48 ~~fractions and nitrate concentrations decrease sharply when flatter landscapes are not able to maintain fast preferential~~  
49 ~~discharge paths (e.g. seepage). The variation of in-stream concentrations, controlled by degradation variability rather~~  
50 ~~than by nitrate source variability, shows a similar three-class response.~~ Our results improve the understanding of nitrate  
51 export in response to topographic slope in a temperate humid climates, with important implications for the  
52 management of stream water quality.

53

54 **Keywords:** topographic slope, coupled surface-subsurface model, young streamflow, in-stream nitrate,  
55 HydroGeoSphere

56

## 57 1 Introduction

58 Globally nearly 40% of land is used for agricultural activities [Foley *et al.*, 2005], which constitutes the major source  
59 of pollution with nutrients such as nitrate (referred as to N-NO<sub>3</sub> in this study). Excess export of nitrate to streams  
60 threatens ecosystem structure and functions, as well as human health via drinking water [Vitousek *et al.*, 2009; Alvarez-  
61 Cobelas *et al.*, 2008; Dupas *et al.*, 2017]. This has been an environmental issue attracting attention in Germany and  
62 world-wide. The dynamics of nitrate export from diffuse nitrogen (N) sources are regulated by the dominant flow  
63 paths that determine the speed at which precipitation travels through catchments before it reaches the stream [Jasechko  
64 *et al.* 2016]. The process is subject to both hydrological and biogeochemical influences mediated by various factors  
65 (e.g. catchment topography, aquifer properties, redox boundaries). From the perspective of sustainable intensification,  
66 process understanding and assessment of potential effects of catchment topography on nitrate export are critical for  
67 the management of water quality in connection with agricultural activity.

68 Field observations in central German catchments indicate that in-stream nitrate concentrations ( $C_D$ ) ~~are show~~  
69 ~~significant differences in the mean concentrations and the seasonal variations generally higher at between~~ downstream

70 areas with gentle topography ~~compared to~~ and more mountainous upstream areas [Dupas et al., 2017; Nguyen et al.,  
71 2022]. This provides strong evidence that catchment topographic slope can influence the nitrate export. In terms of  
72 water age analyses, Jasechko et al. [2016] using oxygen isotope data from 254 watersheds worldwide showed  
73 significant negative correlation between the young (age < 3 months) streamflow fraction and the mean topographic  
74 gradient. They stated that young streamflow is more prevalent in flatter catchments as these catchments are  
75 characterized by shallow lateral flow, while it is less prevalent in steeper mountainous catchments as these catchments  
76 promote deep vertical infiltration. This statistically significant trend is consistent with the common finding that fast  
77 shallow flow paths produce young discharge and potentially ~~promote~~ influence the high in-stream solute  
78 concentrations [Böhlke et al. 2007; Benettin et al. 2015; Hrachowitz et al. 2016; Blaen et al. 2017]. However, apart  
79 from these data-driven analyses, a more mechanistic examination/explanation with the aid of fully resolved flow paths  
80 is still required. Wilusz et al. [2017] used a coupled rainfall-runoff and transit time model to investigate the young  
81 streamflow fraction, with a focus on the effect of rainfall variability rather than on topography and solute export.  
82 Zarlenga et al. [2022] numerically quantified the relative contributions of hillslopes and the drainage network to ages  
83 dynamics in streamflow, considering the influences of transmissivity and recharge, but not without focusing on  
84 topographic slope. The effect of topographic slope on  $C_Q$  has ~~not rarely~~ been subject to systematical testing.

85 Seasonal fluctuation of  $C_Q$  is commonplace in catchments under seasonal hydrodynamic forcing. Field observations  
86 in mountainous central German catchments indicate that nitrate concentrations, as well as the mass load, in streams  
87 vary seasonally, with maxima during the wet winter and minima during the dry summer [Dupas et al., 2017]. Data-  
88 driven analyses by Musolff et al. [2015] and Dupas et al. [2017] suggested the systematic seasonal (de)activation of  
89 N nitrate-source zones as an explanation for such seasonal variability. Under wetter winter conditions the near-surface  
90 N nitrate-source zones in agricultural soils are connected to the stream by fast shallow flow paths. Under drier summer  
91 conditions those nitrate-N source zones are deactivated because their direct hydrologic connectivity to the stream is  
92 replaced with deeper flow paths [Dupas et al., 2017]. Based on high-frequency monitoring in the Wood Brook  
93 catchment in the UK, Blaen et al. [2017] also reported mobilization of nitrate from the uppermost soil layers during  
94 high flow conditions via shallow preferential flow paths, which would not occur during base flow in drier periods.  
95 This behavior leads to a seasonally-variable nitrate loading due to changing flow paths and the associated variation in  
96 transit time that has been observed in many catchments [Benettin et al., 2015; Hrachowitz et al., 2016; Kaandorp et  
97 al., 2018; Rodriguez et al., 2018; Yang et al. 2018]. However, how this fluctuation behaves in response to catchment  
98 land surface topography has not been assessed systematically yet. Such an assessment could improve our  
99 understanding of nitrate export from catchments of different topographic slopes not only in terms of the mean  
100 concentration but also regarding its seasonal-temporal variation patterns bility.

101 Given that most of the above studies used data driven analysis, numerical modeling is an effective tool for the analysis  
102 of water flow, age and solute transport, eliminating the need for large amounts of field data. For example, Van der  
103 Velde et al. [2012] constructed a lumped numerical nitrate transport model for the Hupsel Brook catchment in the  
104 Netherlands, without resolving the spatially-explicit details. Zarlenga and Fiori [2020] presented a physically-based  
105 framework to model the transient water ages at the hillslope scale, which was later used to investigate the different  
106 impacts of hillslopes and the channel network on the water ages in catchments [Zarlenga et al., 2022]. Physically-

107 based hydrogeological models (like, e.g., HydroGeoSphere [Therrien et al., 2010]) resolve the spatially-explicit details  
108 within a catchment including the full variability of 3D flow paths in the subsurface, helping to understand the  
109 seasonally changing flow patterns in response to different catchment topographies. Additionally, the widely used fully-  
110 coupled surface-subsurface technology simulates the catchment as an integrated system, providing details of surface  
111 water-groundwater exchanges fluxes. These details help to identify paths of rapid discharge to the land surface that  
112 can considerably improve the interpretation of nitrate-export patterns.

113 Transit time distributions (TTDs) have been widely used to interpret hydrological and chemical responses in catchment  
114 outfluxes – both in discharge (Q) and in evapotranspiration (ET) [Botter et al., 2010, 2011; van der Velde et al., 2012;  
115 [Heidbüchel et al., 2012](#); Rinaldo et al. 2015; Harman et al., 2015; 2019]. They characterize how a catchment stores,  
116 mixes and releases water as well as dissolved solutes at large spatial and temporal scales [Benettin et al., 2015; Harman,  
117 2015; van der Velde et al., 2010, 2012; Hrachowitz et al., 2015; Van Meter et al., 2017]. Given that the nitrate  
118 attenuation is linked to the age composition of outflow, the TTDs are ideal tools for interpreting the concentration  
119 dynamics with regard to catchment topographic slope. Estimating water ages in natural catchments is still a challenge  
120 due to varying climate conditions, as well as the errors in algorithms (e.g. errors in the flow field during particle  
121 tracking) and limited computational capacity. Yang et al. [2018] used particle tracking to compute the age distributions  
122 in the subsurface of a study catchment (while omitting the 4% of total discharge produced by direct surface runoff and  
123 ignoring the frequent exchange fluxes that may be important for solute export due to their short transit times). [Zarlenga](#)  
124 [et al., \[2022\]](#) used a physically-based semi-analytical model to solve compute the transient water ages in a catchment,  
125 however, without considering the surface run-off and hydrological losses (e.g. ET) being neglected. In this study we  
126 determined the age compositions of Q and ET using numerical tracer experiments, where advective-dispersive  
127 transport of the tracers was solved using the fully-coupled surface-subsurface framework of HydroGeoSphere. The  
128 computed age dynamics based on the tracer concentrations were representative as the tracers were able to track all the  
129 flow processes such as surface runoff, groundwater flow and surface-subsurface interaction.

130 In this study, we attempted to systematically assess the effect of catchment topographic slopes on the nitrate export  
131 dynamics in terms of ~~the mass fluxes~~, concentration levels and its seasonal variability. We also seek mechanical  
132 explanations for the previously found behaviors from data-driven studies (like, e.g., Jasechko et al. [2016]) with the  
133 help of fully resolved flow paths. First, we ~~chose selected~~ a real-world ~~cross section from the~~ small agricultural  
134 catchment ‘Schäfertal’ in Central Germany, which is characterized by strong seasonality in hydrodynamic forcing  
135 with associated shifts in the dominant flow paths [Yang et al., 2018]. This catchment is typical for many catchments  
136 with hilly topography under a temperate humid climate. We created eleven model scenarios by adjusting the mean  
137 slope of the real-world ~~cross section catchment~~ while preserving the ~~land surface micro topography and~~ aquifer  
138 heterogeneity. Next, we modeled the water flow and nitrate transport for each ~~cross section catchment~~. The flow and  
139 transport were solved using the fully coupled surface and subsurface numerical simulator HydroGeoSphere, and the  
140 water ages were computed using numerical tracer experiments. Finally, the modeled flowpaths, water ages, N mass  
141 fluxes and nitrate concentrations under various topographic slopes were analyzed. Through this study, we aimed to (1)  
142 examine the relationship between topographic slope and N mass fluxes, and to (2) assess ~~the  $C_0$  and its~~ seasonal  
143 variation ~~of  $C_0$  and its controls in response to~~ regarding different topographic slopes. ~~The results were supposed to~~

144 ~~improve the understanding of the effects of certain catchment characteristics on nitrate export dynamics with potential~~  
145 ~~implications for the management of stream water quality and agricultural activity.~~

## 147 2 Data collection

### 148 2.1 Real-world and synthetic ~~cross-sections~~catchments

149 Our study was conducted on ~~a vertical cross section selected from~~ the catchment ‘Schäfertal’. ~~This catchment is,~~  
150 situated in the lower part of the Harz Mountains, Central Germany (Figure 12a). The catchment has an area of 1.44  
151 km<sup>2</sup>. The hillslopes are mostly used for intensive agriculture while the valley bottom contains riparian zones with  
152 pasture and a small stream draining the water out of the catchment. The gauging station at the outlet of the catchment  
153 provides Q records. This gauging station is the only outlet for discharging water from the catchment, because a  
154 subsurface wall was erected underneath the gauging station across the valley to block subsurface flow out of the  
155 catchment. A meteorological station 200 m from the catchment outlet provides records of precipitation (J), air and soil  
156 temperatures, radiation and wind speed. The modeled ~~catchment~~cross-section is perpendicular to the stream with a  
157 length of 420 m (Figure 2a, b) and has a mean topographic slope of ~1:20, estimated using a cross-section  
158 perpendicular to the stream (Figure 1a). The aquifer thickness varies from ~5 m near the valley bottom to ~2 m at the  
159 top of the hillslope. Groundwater storage is low (~500 mm) in such a thin aquifer and mostly limited to the vicinity  
160 of the channel with the upper part of the hillslopes generally unsaturated. The stream bed has a depth of 1.5 m below  
161 the land surface, ~~prescribed on the valley side of the cross section~~. Aquifer properties (e.g. hydraulic conductivity)  
162 change from the hillslope, dominated by Luvisols and Cambisols, to the valley bottom, dominated by Gleysols and  
163 Luvisols [Anis and Rode, 2015]. Apart from that, the aquifer generally consists of two layers: the top layer of  
164 approximately 0.5 m thickness with higher porosity and a developed root zone from crops, and the base layer with  
165 smaller porosity due to high loam content [Yang *et al.*, 2018]. Subsequently, ~~six-ten~~ property zones were used (Figure  
166 1b), with zonal parameter values following the model in Yang *et al.*, [2018] listed in Table 1.

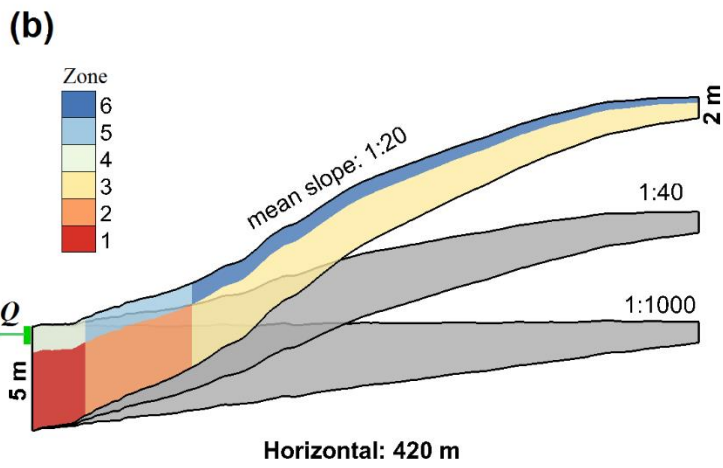
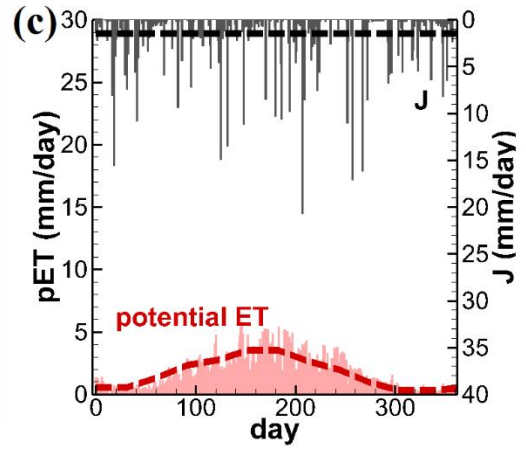
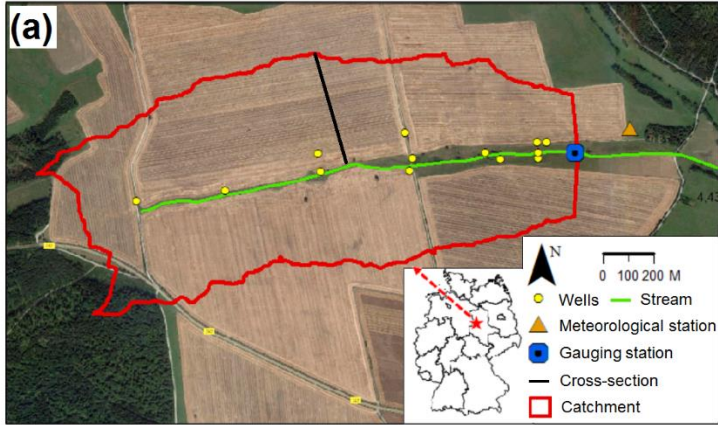
167 Based on this real-world-~~catchment~~cross-sectional aquifer, ten synthetic ~~cross-sections~~catchments were generated by  
168 adjusting elevations (land surface and aquifer bottom), such that the mean topographic slope ranges from 1:20 (steep)  
169 to 1:22, 1:25, 1:30, 1:40, 1:60, 1:80, 1:100, 1:200, 1:500 and 1:1000 (flat, Figure 1b); ~~while preserving t~~The land  
170 surface micro-topography, aquifer depth and heterogeneity were preserved during the adjustments(Figure 1b). In total,  
171 eleven ~~cross-sections~~catchments were used for flow and transport simulations. The catchment with the original  
172 topography (1:20) is selected as the base scenario.

### 174 2.2 Climates

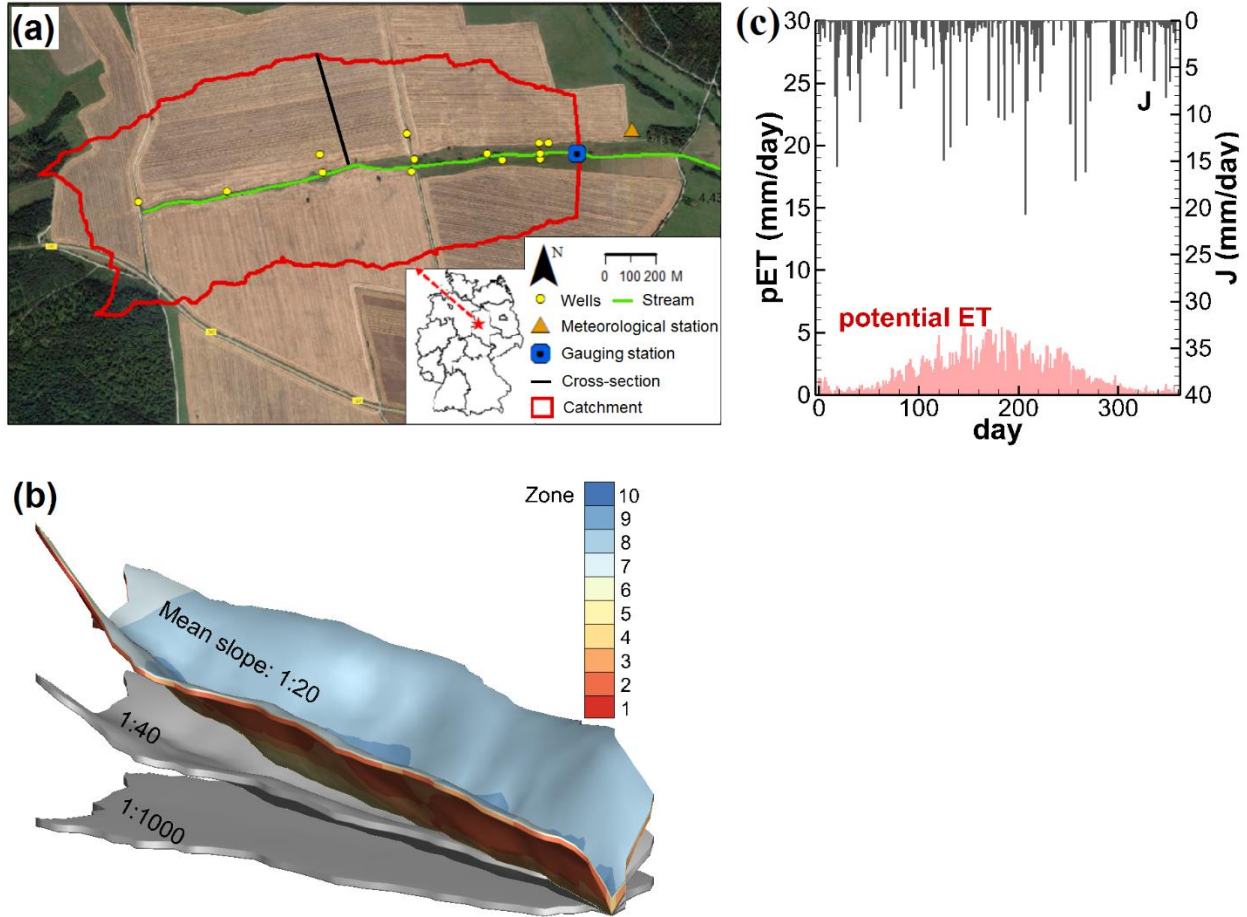
175 The considered climate for the ~~cross-sections~~catchments was derived from the catchment ‘Schäfertal’ located in a  
176 region with temperate humid climate and pronounced seasonality. According to the meteorological data records from  
177 1997 to 2007, the mean annual J and Q (per unit area) are 610 mm and 160 mm, respectively. Actual mean annual ET

178 based on the ten-year water balance ( $J = ET + Q$ ) is 450 mm. Mean annual potential ET is 630 mm [Yang *et al.*, 2018].  
179 The humid climate is representative for wet regions, quantified by an aridity index ( $J / \text{potential ET}$ ) [Li *et al.*, 2019]  
180 of 1.0. The ET is the main driver of the hydrologic seasonality as the precipitation is more uniformly distributed across  
181 the year (Figure 1c). ~~To acknowledge this fact, we selected the data records of the year 2005, and calculated the annual~~  
182 ~~J and monthly averaged potential ET. Using these averaged values in the study can accelerate the simulations and~~  
183 ~~simplify the analysis while preserving the main characteristics of the meteorological forcing to the system.~~

184







186  
 187 **Figure 1.** (a) The catchment ‘Schäfertal’, Central Germany (background image from © Google Maps). (b) The  
 188 The cross-sectional catchments aquifer marked in (a) with a mean topographic slopes of 1:20\_ and two synthetic  
 189 ones with topographic slopes of 1:40 and 1:1000.- (c) The measured precipitation  $J$  and the estimated potential  
 190 evapotranspiration  $ET$  for the year 2005 under the the humid climate [Yang et al., 2018]. Ten aquifer property zones  
 191 in (b) were defined in the subsurface of the catchment for zonal parameter values (e.g. the hydraulic conductivity).  
 192 The dashed lines represent the annual ( $J$ ) and monthly ( $ET$ ) averages.

193

### 194 3 Methods

#### 195 3.1 Flow and nitrate transport

##### 196 Flow model

197 It is necessary to solve both groundwater and surface water flow because the spatially-explicit details in the model  
 198 catchment including the specific flow paths and exchange fluxes are necessary to interpret the effect of varying  
 199 topographic slope on nitrate transport. We simulated the flow system using the fully coupled surface and subsurface  
 200 numerical model HydroGeoSphere, which solves for variably saturated groundwater flow with the Richards’ equation  
 201 and for surface flow with the diffusion-wave approximation of the Saint-Venant equations [Therrien et al., 2010].



202 Additionally, the exchange flux between groundwater and surface water can be implicitly simulated. The nitrate  
203 transport ~~is-is~~ simulated in the groundwater flow, surface flow and exchanges fluxes by solving the advection-  
204 dispersion-diffusion equation describing the conservation of nitrate mass. HydroGeoSphere. ~~The model~~ has been  
205 successfully used to simulate catchment hydrological processes and solute transport in many studies [e.g. *Therrien et*  
206 *al.*, 2010; *Yang et al.*, 2018], therefore governing equations and technical details are not explicitly repeated here.

207 In our previous work *Yang et al.* [2018], a hydrological flow model ~~has~~was already ~~been~~ established for the catchment  
208 ‘Schäferfetal’. It was calibrated against ~~the~~measured groundwater levels and ~~the~~stream discharge Q. The optimized  
209 parameter values are listed in Table 1. In this work, we performed our simulations based on that flow model, with the  
210 nitrate transport process being added ~~while~~ maintaining. ~~However,~~ the model setup ~~is~~ maintained. We provide a brief  
211 review of that flow model here. Readers may refer to *Yang et al.* [2018] for a full description of the model and ~~its~~  
212 calibration.

213 The modeled subsurface of the ~~cross-sections~~catchments was discretized into ~~15-9~~ horizontal ~~element~~layers ~~of~~  
214 ~~prisms~~ between ~~the~~ land surface and ~~the~~ aquifer base, with thinner layers in the upper part (~~--~~0.105 m) to better  
215 represent the unsaturated zone and compute the ET in more detail and thicker layers in the lower part (-1 m). In total,  
216 the subsurface was discretized by a mesh of 13860 prisms, with the horizontal size of the prisms ranging from 30 to  
217 50 m. The cross-sections were 420 m long and uniformly discretized into 200 cells. Apart from that, each cross-section  
218 had a width (lateral direction perpendicular to the cross-section) of 100 m discretized uniformly into 10 cells. The  
219 reason for that was to avoid boundary influences that may have been caused by the lateral flow boundary condition  
220 (described later). In total, the discretization led to 30,000 block elements for the surface. The topmost 2,0001540  
221 triangles ~~-rectangles (200×10)~~ were used to discretize the surface domain, where surface flow was simulated. Ten  
222 property zones for the subsurface were defined (Figure 1b), being assigned with the zonal hydraulic conductivity and  
223 porosity values (Table 1). ET was simulated as a combination of plant transpiration from the root zone (top 0.5 m soil  
224 and evaporation down to the evaporation depth (0.5 m), which are both constrained by soil water saturation. Regarding  
225 the flow boundary conditions, spatially uniform and temporally variable J was applied to the land surface. Spatially  
226 constant and temporally variable potential ET was applied to the aquifer top to calculate the actual ET. The bottom of  
227 the aquifer was considered ~~ans~~ impermeable boundary. A critical depth boundary condition was assigned to the  
228 catchment outlet to simulate the stream discharge Q, which was compared ~~to~~with the measured ~~Qones~~ during the  
229 calibration. The software PEST [Doherty and Hunt, 2010] was used for the transient calibration. After calibration, the  
230 time-variable groundwater levels were well replicated by the flow model for most of the wells, with mean coefficients  
231 of determination ( $R^2$ ) of 0.43. The fit between the simulated and measured Q was satisfactor~~y~~ing with a  $R^2$  of 0.61.  
232 The calibrated model successfully simulated the flow system from 1997 to 2007.

233 In this study, we continued to use ~~the~~ above described model setup, including the mesh, the parameters and the flow  
234 boundary conditions, for the eleven catchments ~~with~~of different topography. Note that the mesh was adapted to the  
235 change of the topography by changing node elevations vertically. However, to simplify the flow simulation and the  
236 age computation (described in section 3.2), we selected the year 2005 as a representative year and assumed~~s~~ that all

237 the years have the identical climate (J and potential ET) as the year 2005. Therefore, the J and potential ET of 2005  
238 (Figure 1c) were cycled and applied to the catchments for all the simulated years.

239

240

241 **Table 1.** The key ~~flow~~aquifer parameters and their values following *Yang et al.*, [2018]. ~~Zonal values are ordered~~  
242 ~~from zone 1 to zone 6.~~

Parameter	Process	Type	Value
Hydraulic conductivity	Subsurface	zonal	2.00, 0.13, 1.18, 0.02, 0.02, 2.00 m day <sup>-1</sup>
Porosity	Subsurface	zonal	0.1, 0.1, 0.1, 0.35, 0.35, 0.35 [-]
Residual saturation	Subsurface	uniform	0.08 [-]
Inverse of air entry pressure $\alpha$	Subsurface	uniform	3.6 m <sup>-1</sup>
Pore-size distribution index $\beta$	Subsurface	uniform	2 [-]
Manning roughness coefficient	Surface	uniform	6.34·10 <sup>-6</sup> day m <sup>-1/3</sup>
Longitudinal dispersivity	Transport	uniform	8 m
Lateral and vertical dispersivity	Transport	uniform	0.8 m
Molecular diffusion coefficient	Transport	uniform	10 <sup>-9</sup> m <sup>2</sup> s <sup>-1</sup>
Degradation coefficient	Transport	uniform	0.009 day <sup>-1</sup>
<b>Transpiration fitting parameters:</b>			
C1	ET	uniform	0.17 [-]
C2	ET	uniform	0.00 [-]
C3	ET	uniform	3.00 [-]
<b>Transpiration limiting saturations:</b>			
Wilting point	ET	uniform	0.1 [-]
Field capacity	ET	uniform	0.2 [-]
Oxic limit	ET	uniform	0.9 [-]
Anoxic limit	ET	uniform	1.0 [-]
<b>Evaporation limiting saturations:</b>			
Minimum	ET	uniform	0.1 [-]
Maximum	ET	uniform	0.2 [-]

Parameter	Process	Type	Value
Hydraulic conductivity	Subsurface	zonal	Zonal values (refer to Yang et al., [2018])
Porosity	Subsurface	zonal	Zonal values (refer to Yang et al., [2018])
Residual saturation	Subsurface	uniform	0.08 [-]
Inverse of air entry pressure $\alpha$	Subsurface	uniform	3.6 m <sup>-1</sup>
Pore-size distribution index $\beta$	Subsurface	uniform	2 [-]
Manning roughness coefficient	Surface	uniform	6.34·10 <sup>-6</sup> day m <sup>-1/3</sup>
Longitudinal dispersivity	Transport	uniform	8 m
Lateral and vertical dispersivity	Transport	uniform	0.8 m
Molecular diffusion coefficient	Transport	uniform	10 <sup>-9</sup> m <sup>2</sup> s <sup>-1</sup>
Degradation coefficient	Transport	uniform	0.009 day <sup>-1</sup>
<b>Transpiration fitting parameters:</b>			
C1	ET	uniform	0.17 [-]
C2	ET	uniform	0.00 [-]
C3	ET	uniform	3.00 [-]
<b>Transpiration limiting saturations:</b>			
Wilting point	ET	uniform	0.1 [-]
Field capacity	ET	uniform	0.2 [-]
Oxic limit	ET	uniform	0.9 [-]
Anoxic limit	ET	uniform	1.0 [-]
<b>Evaporation limiting saturations:</b>			
Minimum	ET	uniform	0.1 [-]
Maximum	ET	uniform	0.2 [-]

244

245

246

### 247 Transport Parameters and boundary conditions for flow

248 The key model parameters for simulating groundwater flow, surface flow and ET are listed in Table 1. Their values  
249 were taken from previous work [Yang et al., 2018], where a hydrological flow model was built and calibrated against  
250 measured groundwater levels and Q for the entire catchment. For each cross section, constant J and time variant  
251 potential ET were applied to the aquifer top. HydroGeoSphere calculates actual ET from potential ET taking into  
252 account the modeled water content, leaf area index and root depth distributions. A free drainage boundary condition  
253 was assigned to the topmost 1.5 m of the subsurface at the valley side (left side) boundary (Figure 1b), enabling  
254 subsurface discharge to the channel. A critical depth boundary [Therrien et al., 2010] was assigned to the left side  
255 edge of the land surface, allowing surface discharge to the channel. In the 3D catchment, surficial flowpaths can  
256 connect the surface water ponding in the depressions of the land surface. In our 2D model, it is unrealistic to force  
257 these surficial flowpaths to be parallel to the cross section. Therefore, our model allowed for the lateral exit of surface  
258 water via the depressions of the land surface by assigning critical depth boundary conditions there. This lateral exit  
259 was also counted as surface discharge to the channel. Finally, the total discharge Q can be calculated by summarizing  
260 the subsurface and surface discharge.

261 ***Parameters and boundary conditions for and parameters transport***

262 The nitrogen (N) pool is formed in the soil zone of the catchments, representing a nitrate source zone. The N pool The  
263 nitrogen pool in the soil is controlled by various complex processes. It is replenished by external inputs from  
264 atmospheric deposition, biological fixation, animal manure from the pasture area, and fertilizer from the farmland on  
265 the hillslopes. Nitrate-N that can be transported with water is formed and leached from this (organic) nitrogen-N pool  
266 by a microbiological immobile-mobile exchange process [Musolff et al., 2017; Van Meter et al., 2017]. In our study,  
267 we employed the simplified framework by Yang et al., [2021] to track the fate of N in the N pool (Figure 2a). This  
268 frame-work was derived/modified from the ELEMent approach (Exploration of Long-tErM Nutrient Trajectories,  
269 Van Meter et al., 2017), which uses a parsimonious modeling framework to estimate the biogeochemical legacy nitrate  
270 loading in the N pool and the N fluxes leaching from the N pool to the groundwater. This framework assumes that  
271 total N load in the N pool is comprised by inorganic N (SIN) and organic N (SON). Two types of SON are  
272 distinguished: active organic N (SON<sub>a</sub>) with faster reaction kinetics and protected organic N (SON<sub>p</sub>) with slower  
273 reaction kinetics. It is assumed that the external N input contributes only to the SON. The SON is mineralized into  
274 SIN. The SIN is further consumed by plants uptake and denitrification, and finally leaches to groundwater as dissolved  
275 inorganic N (DIN, representing mainly nitrate in the studied catchment [Yang et al., 2018; Nguyen et al., 2021]). The  
276 framework is acceptable due to the fact that most of the nitrate fluxes from source zones has undergone  
277 biogeochemical transformation in the organic N pool [Haag and Kaupenjohann, 2001]. The framework simplifies  
278 complexities of different N pools and transformations via mineralization, dissolution, and denitrification within the  
279 soil zone [Lindström et al., 2010], while preserving the main pathway for nitrate leachate.

280 The governing equations to calculate these N fluxes follow the ones in Yang et al., [2021]. A specific portion (*h*) of  
281 the external N input contributes to the SON<sub>p</sub> pool, and the rest contributes to the SON<sub>a</sub> pool. The portion *h* is the land-  
282 use dependent protection coefficient [Van Meter et al., 2017]. The mineralization and denitrification are described as  
283 first order processes with rate coefficients  $k_a$ ,  $k_p$ , and  $\lambda_s$  respectively, using:

$$284 \quad \text{MINE}_a = k_a \cdot f(\text{temp}) \cdot \text{SON}_a \quad (1)$$

$$285 \quad \text{MINE}_p = k_p \cdot f(\text{temp}) \cdot \text{SON}_p \quad (2)$$

$$286 \quad \text{DENI}_s = \lambda_s \cdot \text{SIN} \quad (3)$$

287 where  $\text{MINE}_a$ ,  $\text{MINE}_p$ ,  $\text{DENI}_s$  ( $\text{kg ha}^{-1} \text{ day}^{-1}$ ) are the mineralization rates for SON<sub>a</sub> and SON<sub>p</sub>, and denitrification rate  
288 for SIN.  $k_a$ ,  $k_p$ , and  $\lambda_s$  ( $\text{day}^{-1}$ ) are coefficients for the first order processes.  $f(\text{temp})$  is a factor representing a constraint  
289 by soil temperature [Lindström et al., 2010]. Note that the mineralization and plants uptake occur in the N pool.  
290 Denitrification can occur in both the N pool and later in groundwater. The plants uptake rate UPT follows the  
291 equation used in the HYPE model [Lindström et al., 2010]:

$$292 \quad UPT = \min(UPT_p, 0.8 \cdot \text{SIN}) \quad (4)$$

$$293 \quad UPT_p = p1/p3 \cdot \left(\frac{p1-p2}{p2}\right) \cdot e^{-(DNO-p4)/p3} / \left(1 + \left(\frac{p1-p2}{p2}\right) \cdot e^{-(DNO-p4)/p3}\right)^2 \quad (5)$$

294 where  $UPT$  and  $UPT_p$  ( $\text{kg day}^{-1} \text{ ha}^{-1}$ ) are the actual and potential uptake rates. The computation of  $UPT_p$  considers a  
295 logistic plant growth function.  $DNO$  is the day number.  $p1$ ,  $p2$ ,  $p3$  are three parameters depending on the crop/plant  
296 type, they are in the units of ( $\text{kg ha}^{-1}$ ), ( $\text{kg ha}^{-1}$ ), and (day), respectively.  $p4$  is the day number of the sowing date.



297 The leaching process allows for SIN to leach from the soil (N pool) to the groundwater. The leaching rate  $LEA$  ( $\text{kg}$   
 298  $\text{ha}^{-1} \text{ day}^{-1}$ ) is defined as a first order process as:

$$299 \quad LEA = f \cdot SIN / \Delta t \quad (6)$$

$$300 \quad f = (1 - \exp^{-a \frac{wal}{\theta d}}) \quad (7)$$

$$301 \quad wal = q \cdot \Delta t \quad (8)$$

302 where  $f$  is a factor, ranging between [0, 1], to determine the portion of SIN that leaches into groundwater during a time  
 303 step  $\Delta t$ .  $a$  is unit-less leaching factor.  $\theta$  is the soil porosity.  $d$  is the soil depth.  $wal$  [L] is the water available for  
 304 leaching during  $\Delta t$ .  $wal$  can be estimated using the Darcy fluxes  $q$  [ $\text{LT}^{-1}$ ], which are provided by the flow simulations  
 305 for each cells of the mesh. Physically,  $f$  is a function of the ratio between  $wal$  and the volume of soil voids  $\theta \cdot d$ ,  
 306 representing the ability of water to flush the SIN. This formulation of  $LEA$  is modified from the ones used in  
 307 Pierce et al., [1991], Shaffer et al. [1991] and Wijayantiati et al. [2017], to comply with the spatially-  
 308 distributed HydroGeoSphere model.

309 **Table 2.** The parameters for the N pool and nitrate transport. The parameters with a range are calibrated. The  
 310 adjustable ranges are selected to cover the values that the parameters can potentially reach or the values  
 311 reported by the referred literatures.

<u>Parameter</u>	<u>Description</u>	<u>Range</u>	<u>Reference</u>	<u>Best-fit value</u>
<u>N pool</u>				
$d$	Soil depth	Fixed	Yang et al. [2018]	0.5 m
$N_{Input}$	N external input	Fixed	Nguyen et al. [2021]	180 $\text{kg ha}^{-1} \text{ yr}^{-1}$
$h$	protection coefficient	Fixed	Van Meter et al. [2017]	0.3 [-]
$k_d$	Mineralization coef. ( $\text{DON}_d$ )	[0 - 0.7]	Yang et al. [2021]	0.011 $\text{day}^{-1}$
$k_p$	Mineralization coef. ( $\text{DON}_p$ )	[0 - 0.7]	Yang et al. [2021]	0.0008 $\text{day}^{-1}$
$\lambda_s$	Denitrification coef. (soil)	[0 - 0.7]	Yang et al. [2021]	0.0007 $\text{day}^{-1}$
$p1$	Parameter for plants-uptake	[60 - 160]	Van Meter et al. [2017]	160 $\text{kg ha}^{-1}$
$p2$	Parameter for plants-uptake	[0 - 10]		9.8 $\text{kg ha}^{-1}$
$p3$	Parameter for plants-uptake	[1 - 60]		25.6 day
$p4$	Parameter for plants-uptake	Fixed		63 day
$a$	Leaching factor	[0 - 100]		0.154 [-]
<u>Transport</u>				
$\lambda$	Denitrification coef. (water)	[0 - 0.7]	Yang et al. [2021]	0.0072 $\text{day}^{-1}$
$a_L$	Longitudinal dispersivity	Fixed		8 m
$a_T$	Transverse dispersivity	Fixed		0.8 m

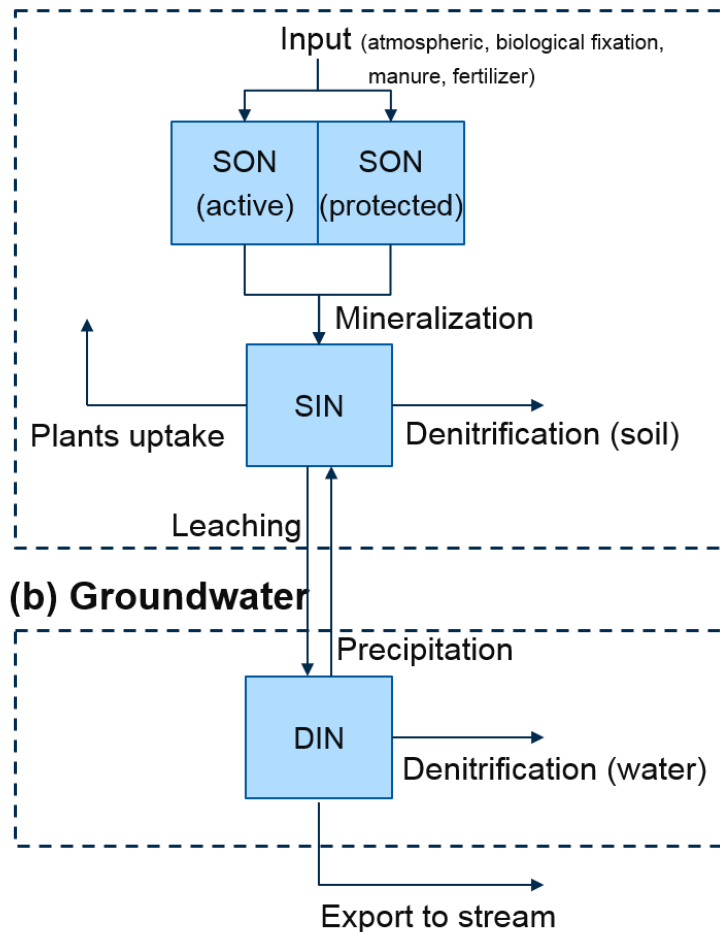
312  
 313 The N pool is positioned on the top part of the aquifer, used as a boundary condition for the DIN (nitrate) transport.  
 314 Advective-dispersive transport of DIN in the flow system is simulated using HydroGeoSphere (Figure 2b). it is not  
 315 necessary to fully implement all the complexities of the different nitrogen pools and transformations into the model,

316 ~~because we focus on the in-stream concentration responses with regard to catchment topography, rather than on the~~  
317 ~~full nitrogen cycle of the catchment. Therefore, we assumed that a nitrate source concentration  $C_j$  was associated with~~  
318 ~~the precipitation. The  $C_j$ , which is time variant, comprehensively defines the amount of dissolved nitrate that can enter~~  
319 ~~the storage along with precipitation. In this study, the  $C_j$  curve followed the time variant nitrate leaching~~  
320 ~~concentrations calculated by *Nguyen et al.*, [2021] using a mesoscale nitrate export model (Figure 2). Additionally,~~  
321 ~~we also considered cases with constant  $C_j$ , which is the average of the time variant values. This constant  $C_j$  was used~~  
322 ~~to quantify the source contribution to the variation of instream concentrations (described in section 3.3). Degradation~~  
323 ~~(denitrification in groundwater) during transport is considered as a first order processes. Degradation is not considered~~  
324 ~~on the land surface (denitrification in surface flow), where ~~the aerobic conditions is more likely to deactivate the~~~~  
325 ~~denitrification and residence time is short.~~

326 To implement the evapoconcentration effect in the transport model, ET is assumed to simplify the transport processes,  
327 ~~theremove -DIN nitrate mass transported with ET (representing plant uptake) was assumed to notwithout altering the~~  
328 ~~nitrate-DIN concentration of the water in storage, and to inject that mass back to the SIN pool. This represents a~~  
329 ~~precipitation process from DIN to SIN, which is thean inverse process of leaching (Figure 2b). There are two reasons~~  
330 ~~for doing that: (i) the physical process ~~ofthat~~ ET causinge the immobilization of DIN can be mathematically considered,~~  
331 ~~and (ii) the N mass balance can be conserved preservedas the plants-uptake is already considered in the N pool~~  
332 ~~according to the plant growth function (Equation 4 and 5), being independent ~~from~~ the ET flux.~~

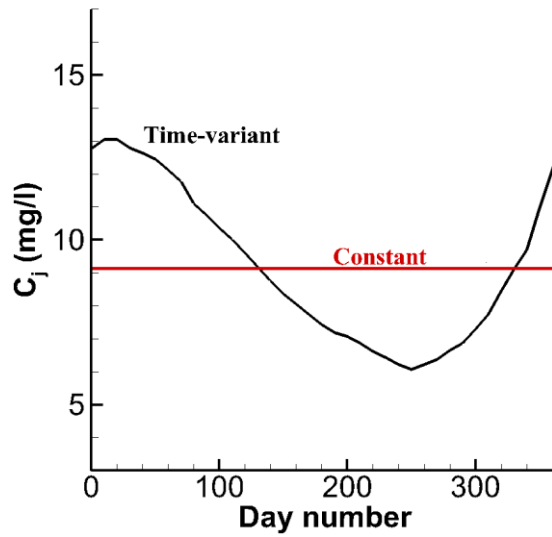
333 Regarding the parameters, the soil depth, within which the N pool is implemented, is set to 0.5 m. N external input is  
334 180 kg ha<sup>-1</sup> yr<sup>-1</sup> according to Nguyen et al. (2021), where the nitrate balance was simulated for the larger upper Selke  
335 catchment ~~(central Germany)~~ that ~~contained~~ vered our studied catchment. The external N input is assumed to be  
336 spatiotemporally constant due to the limited information on its variation in space and time. The protection coefficient  
337  $h$  is fixed as 0.3 according to the values reported in *Van Meter et al.* [2017]. The sowing date  $p4$  is fixed as 63 days  
338 according to the fact that sowing activities and plant growth start in early March. Longitudinal and transverse  
339 dispersivity values were 8 m and 0.8 m, respectively. Other parameters were set to be adjustable and calibrated (Table  
340 2).

### (a) Soil (N pool)



341 ~~neglecting the evapoconcentration~~  
342 ~~effect, because its potential effect to cause source variability was implicitly considered by~~  
343 ~~forcing the source concentration to vary along the  $C_j$  curve. The denitrification in the~~  
344 ~~system was described by the first order decay process with a degradation rate coefficient  $\lambda$~~   
345 ~~of 0.009 day<sup>-1</sup> according to Nguyen et al., [2021] studying the area including the catchment~~  
346 ~~Schäferthal. Longitudinal and transverse dispersivity values were 8 m and 0.8 m,~~  
347 ~~respectively.~~

348  
349



350 **Figure 2.** ~~†~~Conceptual framework for nitrogen (N) fluxes (a) in the soil (N pool), and (b) after leaching into the  
 351 groundwater. ~~he variable and the constant nitrate source concentrations. The constant source is the annual average of~~  
 352 the variable source.  
 353

354 ~~In total, we simulated the flow and transport for 22 scenarios (11 topographic slopes × 2 for variable/constant nitrate~~  
 355 ~~sources). For each scenario, the simulations were run for 100 years with identical boundary conditions for each year.~~  
 356 ~~The first 99 years were used as a spin-up phase to assure a dynamic equilibrium (i.e. to achieve simulated variables,~~  
 357 ~~such as heads and concentrations, being identical between years), and the last year was used for actual observation~~  
 358 ~~and analysis. The CPU time of each simulation was ~4 hours.~~

359  
 360  
 361 **Transport calibration**

362 To get reasonable parameter values for the N pool and N transport, a calibration was performed for the transport. The  
 363 software package PEST [Doherty and Hunt, 2010] was used. In total eight parameters were calibrated (Table 2). Their  
 364 adjustable ranges were selected according to the literatures or to cover the values that the parameters can potentially  
 365 realistically reach. First, the flow and transport were simulated in the catchment of the base scenario (original  
 366 topography, section 2.1), for the period from Jul 1999 to Jul 2003. Secondly, PEST was used to obtain a best fit  
 367 between the simulated results and the data sets by varying the parameter values. We used the measured  $C_0$  and N  
 368 surplus as the data sets. The N surplus, which is the annual amount of N remaining in the soil after consumption  
 369 by plant-uptake, ~~form the external input,~~ was estimated as  $48.8 \text{ kg ha}^{-1} \text{ yr}^{-1}$  (Yang et al., 2021). Note that the simulation  
 370 period from Jul 1999 to Jul 2003 was only used for model calibration, rather than for the actual simulations with the  
 371 eleven catchments of different topographic slope. After calibration, the model with the best-fit parameter values can  
 372 well replicate the measured  $C_0$  with a Nash-Sutcliffe efficiency (NSE) of 0.75 (see Figure S1 in the supporting  
 373 information). The simulated N surplus was  $50.7 \text{ kg ha}^{-1} \text{ yr}^{-1}$ , being comparable to ~~with~~ the measured value.

374 The best-fit parameter values were also used for the catchments of different topographic slope, assuming that the  
375 parameters do not change with the change of topographic slope. In total, we simulated the flow and nitrate transport  
376 for eleven scenarios (11 catchments of different topographic slope). For each scenario, the simulations were run for  
377 100 years with identical boundary conditions for each year. The first 99 years were used as a spin-up phase to assure  
378 a dynamic equilibrium (i.e. to achieve simulated variables, such as heads and concentrations, that are being identical  
379 between years), and the last year was used for actual observation and analysis. The CPU time of each simulation was  
380 ~4 hours.

381

### 382 3.2 Water ages

383 The water stored in a catchment (storage), Q and ET can all be characterized by ~~its~~ age distributions, for they ~~it~~  
384 ~~comprises~~ water parcels of different age from precipitation events that occurred in the past. The age distributions need  
385 to be calculated for each aforementioned scenario to assess the responses of water ages on catchment topographic  
386 slope. Our model setup (with virtual ~~cross-sections~~ catchments and identical climate for each year) allowed us to  
387 perform long-term numerical tracer experiments and to extract the age distributions.

388 We assumed that inert tracers of uniform concentration existed in precipitation. The tracers were applied to the land  
389 surface as a third-type (Cauchy) boundary condition and were subjected to transport modeling. Tracer can exit the  
390 aquifer via the outfluxes Q and ET. We considered a period of 200 years for the tracer experiments, which was  
391 sufficiently long to ensure convergence of the computed water ages. The 200 years period was partitioned into 2400  
392 months ( $\Delta t = 1$  month). A different tracer was used for each of the periods resulting in a total of 2400 distinct tracers.  
393 The injection of tracer  $i$  started with the precipitation at the beginning of its associated period  $t_0^i$  and lasted throughout  
394 the period ~~with the precipitation~~. The advective-dispersive multi-solute~~s~~ transport was simulated using  
395 HydroGeoSphere. The first 199 years of the simulation period were used as a spin-up phase to ensure a dynamic  
396 equilibrium of the calculated ages, minimizing the influence of the initial conditions. The last year was used for the  
397 actual observations and the computation of age distributions. Solving the transport of the 2400 tracers ~~is~~ would be  
398 computationally expensive. However, because the climate (flow boundary conditions) was identical for each year, the  
399 transport simulation was performed only for the first 12 tracers that covered the course of a year. Based on these  
400 results, the results for the other 2388 tracers were manually reproduced (e.g., by shifting the concentration  
401 breakthrough curves of the 12 tracers in time while maintaining the shapes).

402 For each tracer, the breakthrough curves of the mass-fluxes of Q and ET, as well as the mass in storage were reported.  
403 For a specific time  $t$ , the age distributions for Q/ET/storage were computed by calculating the mass fraction of each  
404 tracer using:

$$405 \quad p_{Q/ET/S}(T, t) = \frac{M^i(t)}{\Delta t \sum M^i(t)} \quad (9)$$

406

407 where  $p_Q(T, t)$ ,  $p_{ET}(T, t)$  are the age distributions of Q, ET (equivalent to backward transit time distributions - TTDs),  
408 and  $p_S(T, t)$  is the age distributions of water in storage (equivalent to the residence time distribution - RTD).  $M^i(t)$  is

409 the mass-flux of the tracer  $i$  in Q or ET, or the mass stored in catchment at time  $t$ ,  $\sum M^i(t)$  is the sum of  $M^i(t)$  over  
410 all tracers.  $T$  is the age ranging within  $[t - t_0^i - \Delta t, t - t_0^i]$  that equals  $t$  — for tracer  $i$ .

411 For each scenario, the CPU time of the tracer experiment was ~8 hours. Based on the age distributions, we calculated  
412 the mean discharge age  $T_Q(t)$ , which is equivalent to the mean discharge transit time (simply referred to as ‘discharge  
413 age’ in the following sections). We calculated the young water fraction in streamflow  $YF_Q(t)$ , which is the fraction of  
414 streamflow with an age younger than three months (also referred to as ‘young streamflow fraction’ [Jasechko *et al.*  
415 2016]). Similarly, the ET age  $T_{ET}(t)$  and the young water fraction in ET  $YF_{ET}(t)$  can be calculated as well (more  
416 details are described in Text S1 of the supporting information). Their responses to ~~a~~ changes in topographic slope  
417 were analyzed.

418

### 419 **3.3 Assessment variables**

420 ~~The simulations of flow, nitrate transport and water age provided in stream nitrate concentrations ( $C_f$ ), streamflow ages~~  
421 ~~( $t$ ) and young water fractions  $YF(t)$  for each scenario. They all fluctuated seasonally over the course of a year. The~~  
422 ~~temporal means and standard deviations  $\sigma$  of these variables can be calculated. The temporal variation in can~~  
423 ~~potentially be split and attributed to (i) the variability in the nitrate source concentration, referred to as source~~  
424 ~~contribution, and (ii) the variability created by degradation associated with variable transit times, referred to as~~  
425 ~~degradation contribution. To understand which of these processes has the dominant effect on  $C_f$  variability, we~~  
426 ~~quantified the source contribution by calculating the relative change of  $\sigma$  for when  $C_f$  switches from being time-variant~~  
427 ~~to being constant between separate model scenarios (see section 3.1), as:~~

$$428 \text{Source contribution} = 1 -$$

429 ~~The calculated source contribution ranges from 0 (degradation dominated) to 100 % (source dominated). Additionally,~~  
430 ~~the Damköhler number ( $Da = \lambda \cdot T$ , [Oldham *et al.*, 2013]), which is a dimensionless ratio between the discharge age~~  
431 ~~and the reaction time, can be calculated to indicate the interplay between the rate of degradation and the time scale of~~  
432 ~~transport.  $Da > 1$  indicates a faster degradation time than transport time and vice versa.~~

433

## 434 **4 Results and discussion**

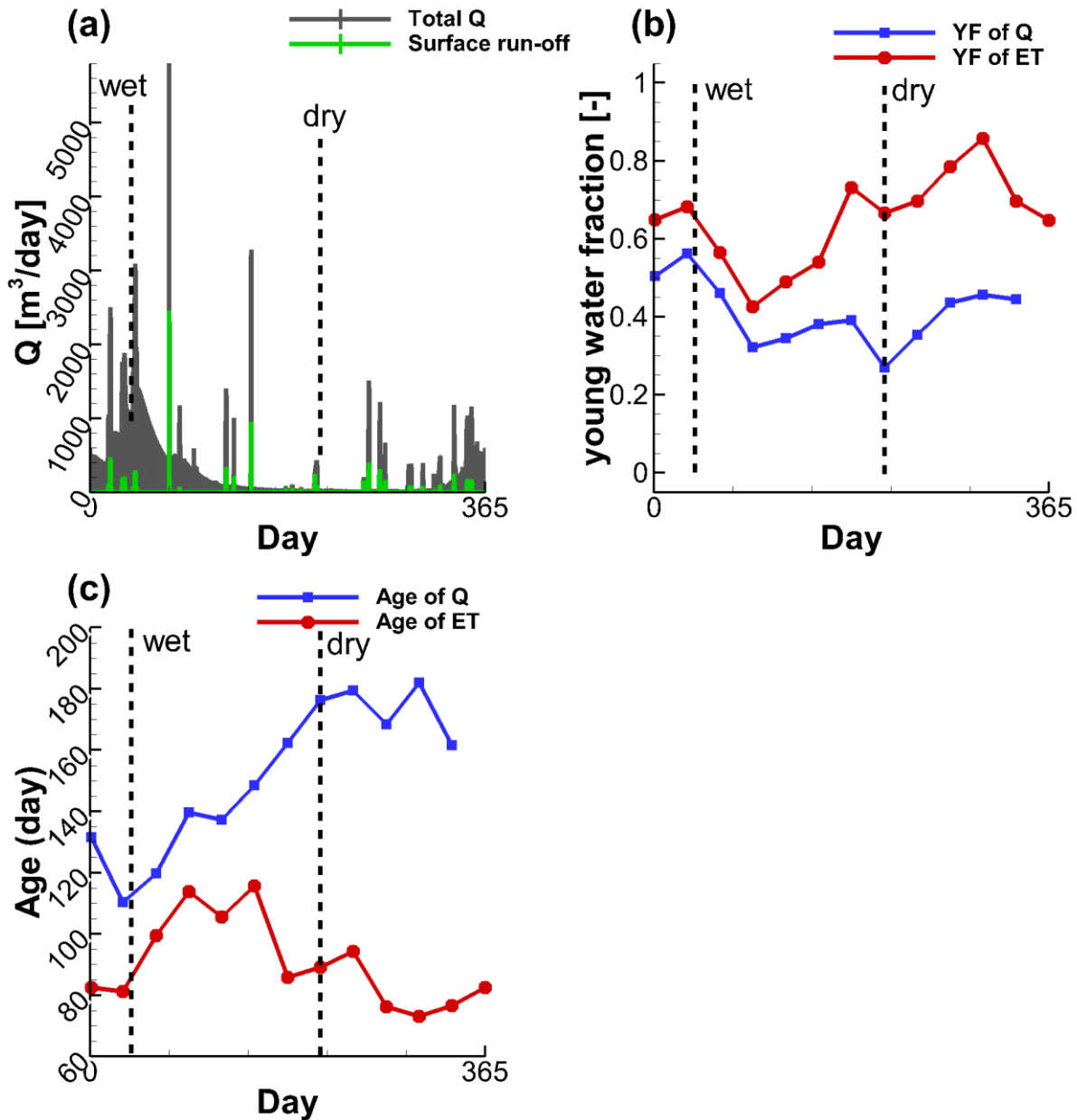
### 435 **4.1 Dynamics of water ages and nitrogen fluxes**

436 ~~For all the scenario~~ Driven by the seasonality of the climate of seasonality, the simulated Q, in in-stream nitrate  
437 concentrations  $C_f$ , the young water fractions  $YF$ , and the water ages all show seasonal fluctuations. Figure 3 shows  
438 these fluctuations for the base scenario (original cross section with topography) ie slope of 1:20. Q reaches its  
439 maximum towards the end of the wet winter in late February and reaches its minimum during the drier late summer  
440 in mid-September. Total Q consists of a portion of groundwater discharge (including the flow via vadose zone) and a  
441 portion generated via surface-runoff during events of high precipitation (Figure 3a). The calculated For  $YF_{ET}$  (Figure  
442 3b) show that  $C_f$ , high concentrations are reached during the wet season and low concentrations are reached during



443 ~~the dry season (Figure 3b). Figure 3c depicts opposing fluctuation patterns of  $YF_Q$  and  $YF_{ET}$ .~~ Young water fraction in  
444 ET is smallest~~reaches the lowest in April and largest~~the highest in November (Figure 3b), is low during the wet and  
445 high during the dry season, while  $YF_Q$  young water in Q reaches~~is the smallest~~lowest in August and largesthighest  
446 in February~~during the dry and high during the wet season.~~ ET generally has larger young water fractions than Q as ET  
447 has a higher probability to remove young water from the shallow soil rather than the older water ~~from~~from the deeper  
448 aquifer. Especially during the dry season (summer), most precipitation can be quickly removed by ET. The water ages  
449 of Q and ET show generally opposite fluctuation patterns for~~against~~  $YF$  (Figure 3c). ~~d shows that~~ The ET age ranges  
450 from 192-70 to 395-115 days, being younger than Q that has the age ranging ~~older during the wet and younger during~~

451 the dry season. Simulated discharge age ranges from 125-109 to 149-180 days, being younger during the wet and  
 452 older during the dry season.



453  
 454 **Figure 3.** Simulated (a) Q, (b) young water fractions in streamflow ( $YF_Q$ ) and evapotranspiration ( $YF_{ET}$ ),  
 455 and (c) water ages for the catchment of the base scenario. The YF and water ages are monthly averaged.

456  
 457 The simulated  $C_O$  shows strong seasonality with the maxima are reached in the wet period and the minima are reached  
 458 in the dry period, fitting the measured  $C_O$  data well (Figure 4a). Figure 4b lists the calculated annual N mass balance  
 459 in the catchment of the base scenario. The organic (SONa + SONp) and inorganic (SIN) N load in the soil are 470 kg  
 460 ha<sup>-1</sup> and 43 kg ha<sup>-1</sup>, respectively. The SON accounts for 92% of the total N load, which is consistent with the study of

461 Stevenson [1995] where the organic N fraction was reported to be greater than 90%. The mineralization converts  
462 SON into SIN with a rate of 180 kg ha<sup>-1</sup> yr<sup>-1</sup>. This rate is equal to the external N input because this way at the steady-  
463 state of the annual N mass balance was reached in the simulations. About 76% of the input N flux is taken up by the  
464 vegetation plant (136 kg ha<sup>-1</sup> yr<sup>-1</sup>). 20% is consumed by denitrification (36 kg ha<sup>-1</sup> yr<sup>-1</sup>), either in the soil (before  
465 leaching) or into the groundwater (after leaching). The remaining 4% reaches the stream water and is exported out  
466 of the catchment (6 kg ha<sup>-1</sup> yr<sup>-1</sup>). The simulated mineralization flux is within the range of [14–187] kg ha<sup>-1</sup> yr<sup>-1</sup> reported  
467 by Heumann et al. [2011] for their study sites in central Germany. The simulated plant uptake and leaching fluxes are  
468 comparable to the values suggested in Nguyen et al. [2021] for the same area (120 kg ha<sup>-1</sup> yr<sup>-1</sup> for plant uptake and  
469 [15–60] kg ha<sup>-1</sup> yr<sup>-1</sup> for leaching). The simulated denitrification rate is within the range [8–51] kg ha<sup>-1</sup> yr<sup>-1</sup> reported in  
470 Hofstra and Bouwman [2005] for 336 agricultural soils located worldwide. Moreover, 80% and 20% of the  
471 leaching N are consumed by denitrification during transport in the groundwater and exported to stream water,  
472 respectively. These portions are generally comparable to those reported in Nguyen et al. [2021] (61% and 39%,  
473 respectively). Therefore, the simulated N loads and fluxes for the catchment of the base scenario are considered to be  
474 acceptable.

475 Figure 4c shows the temporal variation of the N load and fluxes. It demonstrates that low levels of SIN are maintained  
476 by high plant-uptake before the dry summer arrives (May – June), such that there is little SIN available for leaching.  
477 The SIN load reaches its minimum when plant uptake reaches its maximum (marker a in Figure 4c). The cessation  
478 of plant-uptake during the dry period leads to the increase of the SIN load as well as the increase of the leaching rate.  
479 The mineralization in winter is significantly reduced due to the dropping temperatures, cutting the SIN supply. This  
480 results in that the SIN load reaches its high peak in the middle of November (marker b in Figure 4c) and  
481 subsequently turns into the dropping decrease phase due to increased leaching and eventually plants uptake. These  
482 seasonal fluctuation patterns are generally consistent with the knowledge of N fluxes reported in previous studies  
483 [Dupas et al., 2017; Nguyen et al., 2021]. For DIN load in water, it reaches its maximum generally when the  
484 leaching becomes weakens in the beginning of March (marker c in Figure 4c), and reaches the minimum just before  
485 the leaching process becomes active again in the end of August (marker d in Figure 4c). These low and high peaks of  
486 SIN and DIN loads can also be identified by their spatial distributions in the catchment (see Figure S2 in the supporting  
487 information).

## 488 **4.2 In-stream nitrate seasonal variations**

489 Simulated results demonstrate significant seasonal variations of  $C_O$  for all the scenarios (Figure S2 in the  
490 supporting information). Basically, this variation in  $C_O$  can be directly influenced is caused either by the fluctuation  
491 of the nitrate source input leaching into groundwater, or by fluctuations in the degradation in groundwater  
492 associated with the varying transit times (quantified by the young water stream fraction in streamflow  $YF_O$ ). These two  
493 influences represent the effect from the variability in N source and in N transport, respectively. Linear regression  
494 analysis shows that  $C_O$  is correlated with leaching flux rate and  $YF_O$  with Spearman rank-correlation coefficients of  
495 0.1 and 0.34, respectively (Figure 5). The seasonal fluctuations of  $C_O$  and leaching flux are temporally out of phase.  
496 The maximum leaching occurs reaches in December, while the maximum  $C_O$  is reacheds two months later in February

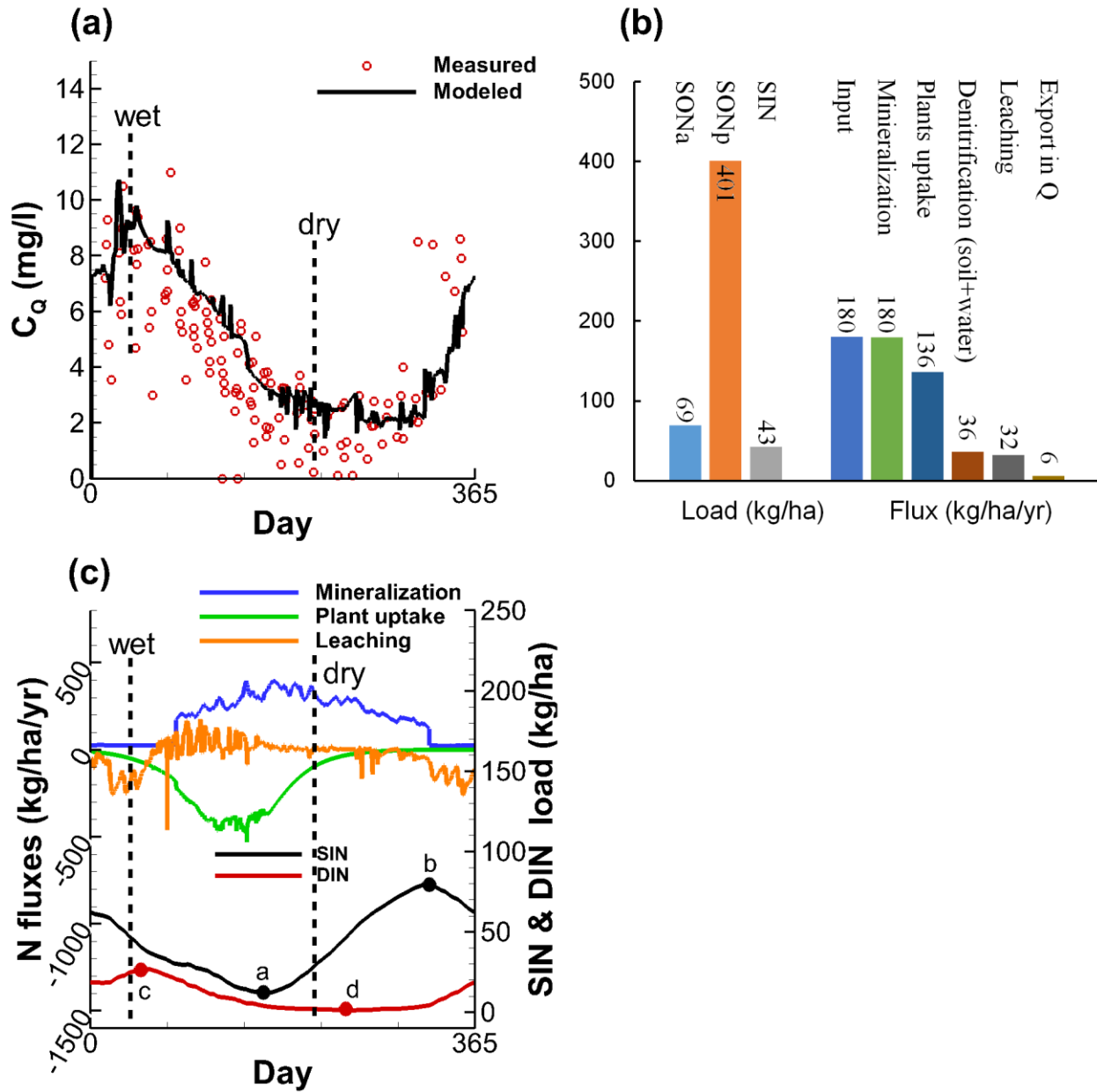
497 (Figure 5a). The minimum leaching ~~occurs~~reaches in April, while the minimum  $C_Q$  is reacheds around September.  
498 This behavior indicates that  $C_Q$  respondse later to the changes in N leaching, which is reasonable because the leaching  
499 nitrate needs time to travel from the shallow soil to streamflow. The fluctuation of ~~the~~ $C_Q$  and  $YF_Q$  are more  
500 synchronized, provened by the fact that both maximaums are reacheds in February (wet, Figure 5b) and minimaums  
501 ~~occur~~reaches generally in ~~the~~ dry summer time. Field observations in mountainous central German catchments also  
502 indicate that  $C_Q$  variesy seasonally, with maxima during the wet winter and minima during the dry summer [Dupas et  
503 al., 2017]. These seasonal fluctuations of  $C_Q$  and  $YF_Q$  were frequently explained using the “inverse storage effect”  
504 [Harman, 2015; Yang et al. 2018]: during the wet season Q has a strong preference for young water associated with  
505 higher concentrations, which would not occur during dry periods due to the deactivation of the shallow fast flow  
506 processes. These patterns generally suggest that ~~The calculated source contribution for our simulated scenarios~~  
507 indicates that only 2 to 33 % of the variation of  $C_Q$  can be attributed to the fluctuation of source concentrations (Figure  
508 8a). This means that the  $C_Q$  nitrate concentration fluctuation is more attributed to s in all simulated cross sections are  
509 dominated by the variability in ~~the N transport~~degradation time (transit time) rather than to the variability in the N  
510 source, echoing with previous observations that 80%% of the leaching N mass is degraded during transport. However,  
511 it is still hard to tell whether the N source or the N transport is dominating the  $C_Q$  fluctuation.

512 ~~In other words, significant seasonal variation of the nitrate concentration in streamflow can be expected under the~~  
513 ~~considered humid climate even when nitrate is applied to the aquifer in a constant manner without any variation. These~~  
514 ~~seasonal fluctuations of transit time and  $C_Q$  were frequently explained using the “inverse storage effect” [Harman,~~  
515 ~~2015; Yang et al. 2018]: during the wet season Q has a strong preference for young water associated with higher~~  
516 ~~concentrations, which would not occur during dry periods due to the deactivation of the shallow fast flow processes.~~  
517 ~~This effect was revealed in the computed TTDs for Q indicated by the shift between wet and dry seasons (Figure S3~~  
518 ~~in the supporting information).~~

519 ~~The response of the source contributions to topographic slope is threshold like (Figure 8a): the source contributions~~  
520 ~~in C1 were significantly higher than the ones in C3. Especially for the landscapes of C3, the fluctuation of  $C_Q$  was~~  
521 ~~hardly impacted by source variability. Mechanically, the seasonal source fluctuation is more likely to be damped by~~  
522 ~~relatively longer transit times in C3 landscapes, which are relatively flat.~~

523 ~~Given that the seasonal  $C_Q$  variation can be attributed more to the variation in transit times (thus to the variation in~~  
524 ~~the  $YF_Q$ ), it was expected that the standard deviations of  $C_Q$  and  $YF_Q$  (Figure 8b, e) had similar responses to the~~  
525 ~~topographic slope. Both of the responses exhibit a threshold like pattern, similar to the response of the mean  $C_Q$~~   
526 ~~(Figure 4a). This is because  $C_Q$  during the dry season is generally low, regardless of whether the landscape is steeper~~  
527 ~~or flatter. The overall response of  $\sigma(C_Q)$  to topographic slope is determined by the response of the relatively high  $C_Q$~~   
528 ~~during the wet season, and can be interpreted in the same three class pattern:  $\sigma(C_Q)$  increases with the decrease of~~  
529 ~~slope within C1 (or C3), suggesting that flatter landscapes tend to export nitrate with more seasonal fluctuations in~~  
530  ~~$C_Q$  for C1 (or C3). However, for C2, a significant drop in this fluctuation can be expected when the landscape~~  
531 ~~transforms from C1 to C3. As a result, the maximum seasonal variation was reached at the slope of 1:60. For the~~  
532 ~~mechanistic interpretation please refer to section 4.1.~~

533 ~~Generally, the seasonal fluctuation patterns of  $C_Q$ , with both variable source and constant source, are highly~~  
534 ~~correlated with the fluctuation pattern of the  $YF_Q$  with Spearman rank correlation coefficients of 0.81 and 0.93,~~  
535 ~~respectively. The calculated  $Da$  for streamflow is 13, demonstrating that the degradation time scale is significantly~~  
536 ~~shorter than the transport time scale. This means young streamflow is the main contributor of nitrate mass as most of~~  
537 ~~the nitrate in the older water has been degraded before reaching the stream.~~

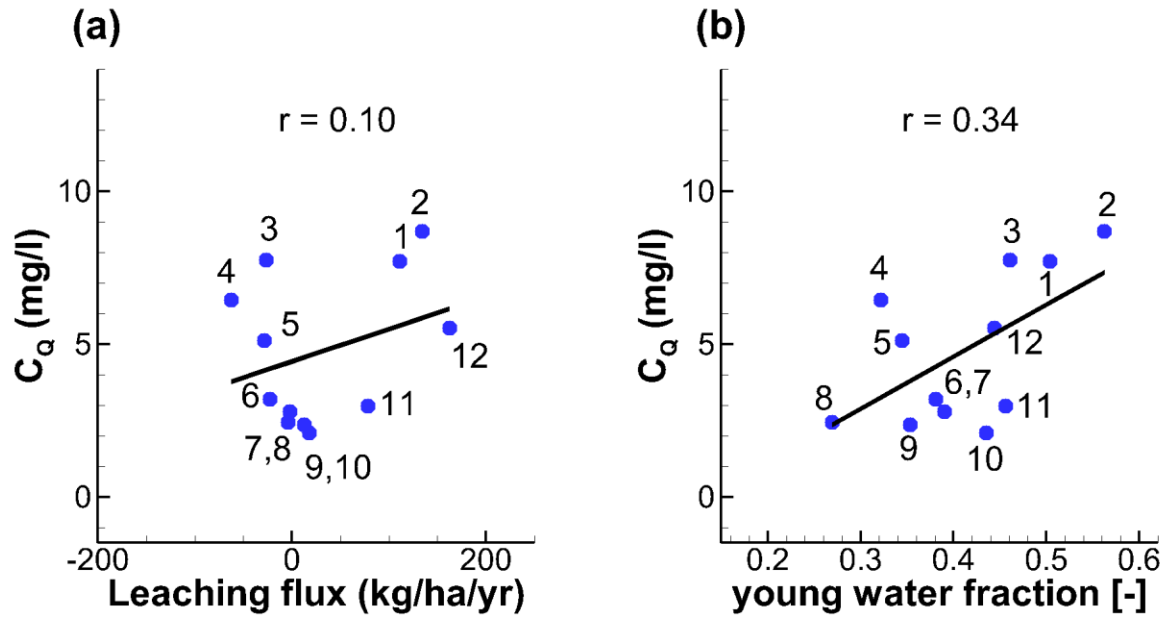


539

540 **Figure 4.** Simulated (a) In-stream nitrate concentration  $C_Q$ , (b) N loads and fluxes, and (c) time-variable N fluxes for

541 the catchment of the base scenario. Note that the measured  $C_Q$  in (a) includes all the measurements from 2001 to 2010.

542



543

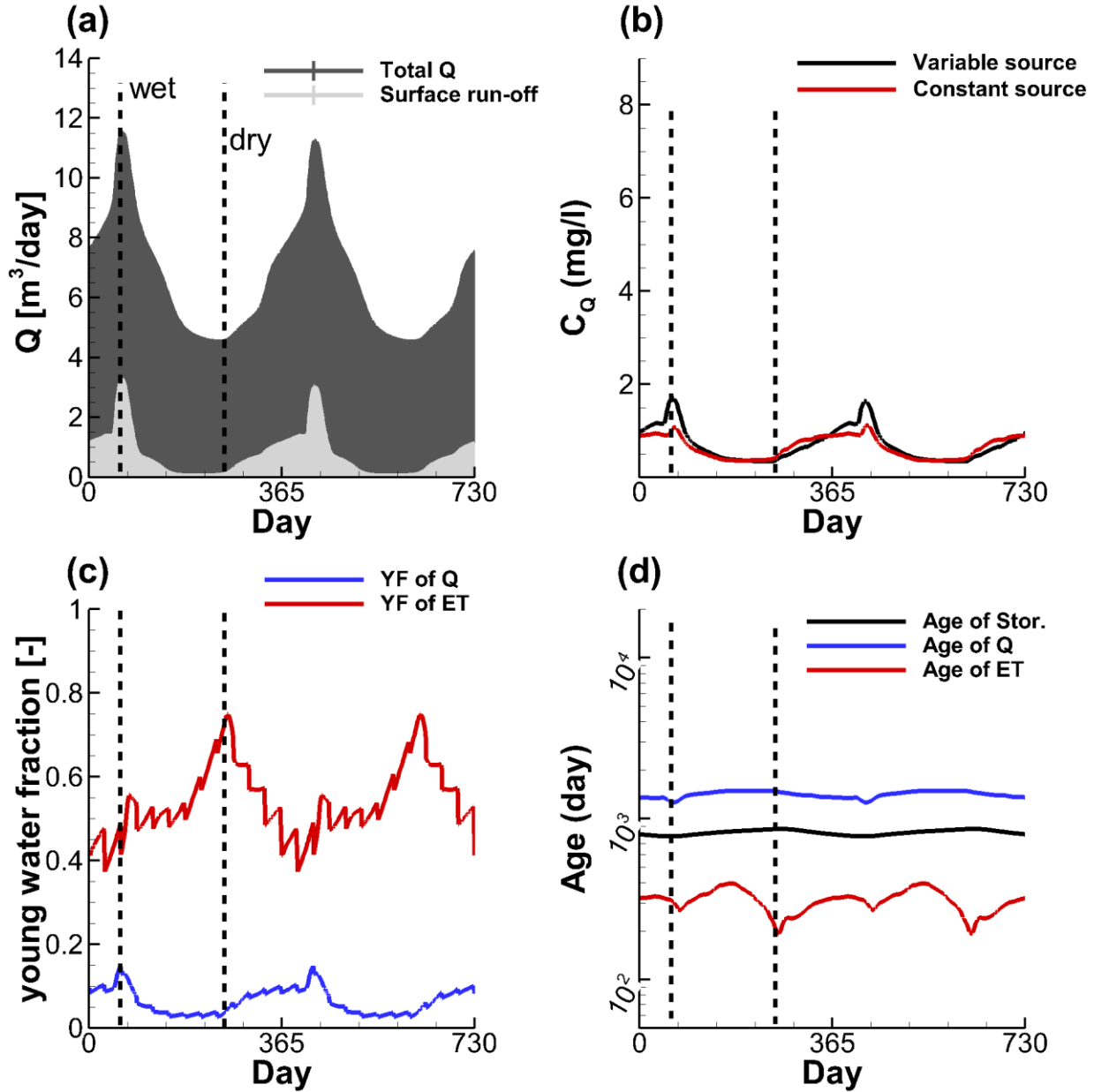
544

545

546

**Figure 5.** Comparing the monthly averaged  $C_q$  with (a) the leaching flux and (b) the young water fractions of Q. The black lines are linear fits of the two variables with linear relationship, with  $r$  being the Spearman rank-correlation coefficient. The numbers are referred to the months.





548

549

550

**Figure 3.** Simulated (a)  $Q$ , (b) in-stream nitrate concentration  $C_Q$ , (c) young water fractions  $YF_Q$  and  $YF_{ET}$ , and (d) water ages for the cross-sectional aquifer with topographic slope of 1:20.

551

552

#### 4.21 Effect of topographic slope on flow In-stream nitrate level

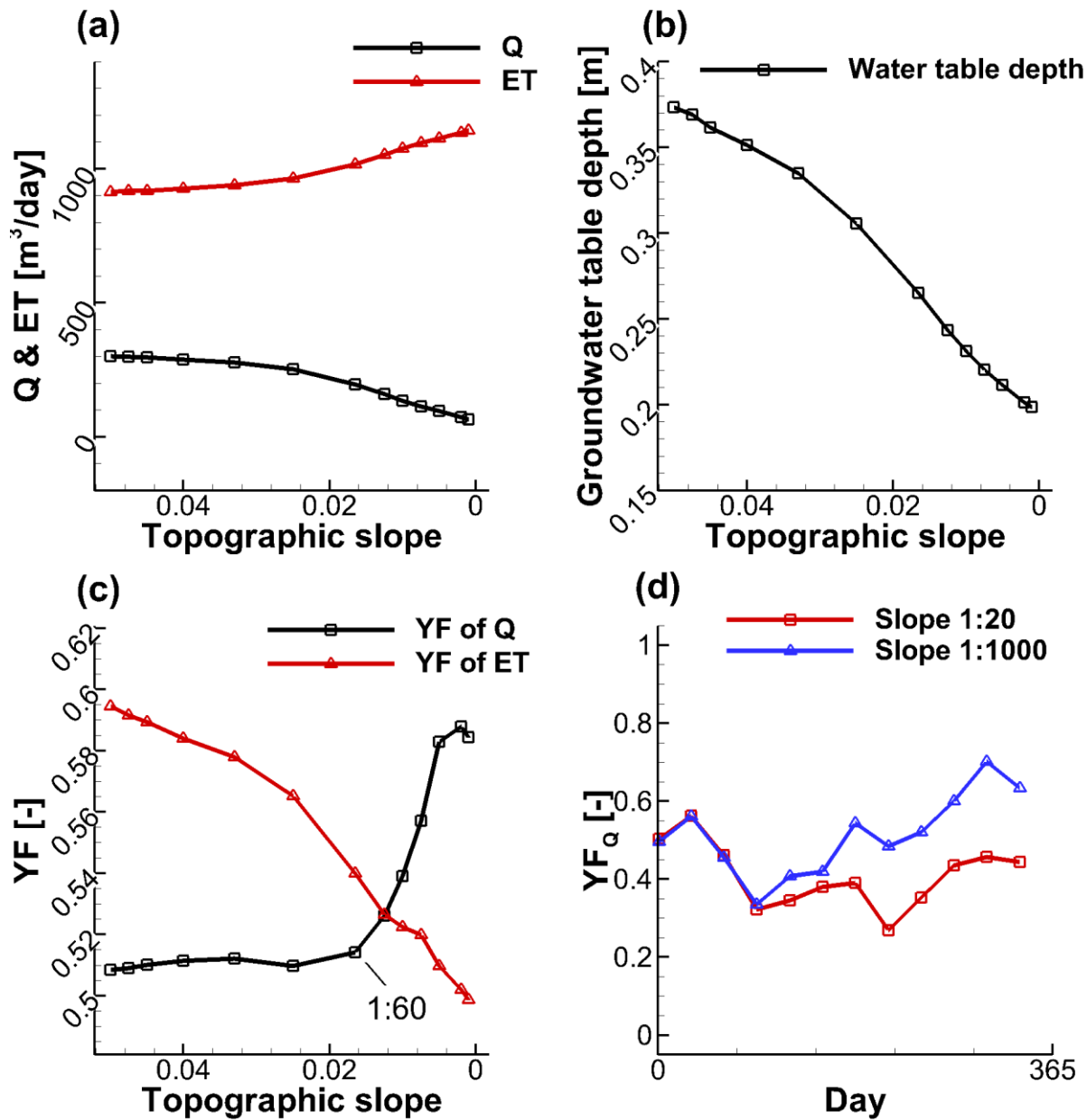
553

554

555

With the help of our simulations, it is possible to systematically explore the influence of topographic slope on the water flow and N fluxes concentrations of nitrate exported to the stream. Figure 6 shows For each scenario with time-variant nitrate source concentration, we analyzed the responses of temporally-averaged mean- $Q$  and ET, the

556 groundwater table depth, and flow weighted mean  $YF_Q$  and  $YF_{ET}$  to the changes of topographic slope,  $C_Q$ , as well as  
557 the  $C_Q$  extracted at a wet time and a dry time (marked with the dashed line in Figure 3b). Under a constant ~~unchanged~~  
558 climate, the changes of topographic slope can reshape the water flow via influencing flow partitioning between  
559 ~~Q discharge~~ and ET. More water is taken up by ET and less water becomes ~~by Q~~ in flatter landscapes (Figure 6a). These  
560 patterns can be explained by the change of groundwater table depth (Figure 6b), as shallower groundwater tables can  
561 be reached by the vegetation in flatter landscapes where ET therefore has a higher chance to remove water from the  
562 subsurface. The simulated  $YF_Q$  and  $YF_{ET}$  show generally increasing and decreasing patterns, respectively, when the  
563 topographic slope decreases (Figure 6c), demonstrating that young streamflow is more prevalent in flatter landscape  
564 and young ET is more prevalent in steeper landscapes. However, the increasing pattern of  $YF_Q$  ~~is does not~~  
565 ~~continue pronounced in the~~ steep catchments with ~~the~~ slopes  $> 1:60$ . Topographic slope ~~has changed the~~  $YF_Q$  not only  
566 in terms of its mean value, but also in terms of ~~its~~ the temporal variations. Figure 6d indicates that the maximum and  
567 minimum  $YF_Q$  are reached in February and August for the steepest catchment (slope 1:20), respectively, ~~and however,~~  
568 in November and April for the flattest catchment (slope 1:1000).



570

571 **Figure 6.** The simulated (a) Q and ET, (b) spatially-averaged depth of the groundwater table from the land surface,  
 572 (c) young water fraction in streamflow  $YF_Q$  and evapotranspiration  $YF_{ET}$ , in relation to the topographic slope for  
 573 the simulated catchments. (d) compares the temporal variations of time-variable  $YF_Q$  between for a steep landscape  
 574 (slope 1:20) and a flat land scape (slope 1:1000).

575

576

577 ~~Interpreting the three-class response of the  $YF_Q$  to topographic slope~~ mechanistically requires a closer  
578 look at the flow processes ~~using with~~ in the cross-sectional views. We plotted the subsurface flow fields ~~for the~~  
579 ~~the\_~~ wet season ~~at for the a~~ cross-sections of the catchments with slopes 1:20, 1:60, 1:100, and 1:1000 (Figure 75).

580  
581 ~~(1) For C1 (slope 1:20 — 1:60),~~ Figure 75a reveals that the hillslope part of the aquifer-catchment with a slope of 1:20  
582 is largely unsaturated so that the flow paths in this area are characterized by vertical infiltration ~~(Figure 5a)~~. In contrast,  
583 the valley bottom is fully saturated. Overall, 34% of the subsurface domain ~~(in volume)~~ is characterized by vertical  
584 flow (flow in 34% of the total aquifer volume is more vertical than horizontal). For this scenario two main discharge  
585 routes to the stream can be identified: (i) A fraction of the groundwater flows through the fully saturated zone and  
586 exits the aquifer to the stream, and (ii) another fraction exits the aquifer via seepage near to where the groundwater  
587 table intersects the land surface, indicated by a large exchange flux (from subsurface to surface, positive). The seepage  
588 represents a preferential flow path allowing for rapid discharge via overland flow instead of slower discharge via the  
589 sub-surface with longer transit times. Note that both of the discharge routes provide the pathways for the rainfall  
590 falling on the top hillslope to reach the stream.

591 When the slope is reduced to 1:1000, the flow pattern experiences significant changes (Figure 7b) compared to  
592 with the catchment with a slope of 1:20.

593 ~~(2) For C2 (slope 1:60 — 1:100), even though the groundwater table depth is still decreasing with decreasing slope,~~  
594 ~~the flow pattern experiences a rapid change. The seepage flow vanishes because the groundwater table (fully or~~  
595 ~~partially) disconnects from the land surface (Figure 5c). The water that would have flown to the stream via seepage~~  
596 ~~has to take slower flow paths in the subsurface to the valley bottom. The surface run off dropped significantly from~~  
597 ~~7.1 m<sup>3</sup>/day to 0.5 m<sup>3</sup>/day (Figure 5c, d). Basically, decreasing the topographic slope reduces the horizontal component~~  
598 ~~of the hydraulic head gradients, which is obvious as part of the precipitation falls at lower elevations instead of farther~~  
599 ~~up the hillslope. The reduced head gradient generally slows down the groundwater flow velocity.~~

600 Several hydrologic studies have described two different flow systems in aquifers: (i) a recharge-limited system where  
601 the thickness of the unsaturated zone is sufficient to accommodate any water-table rise and thus the elevation of the  
602 groundwater table is limited by the recharge, and (ii) a topography-limited system where the groundwater table is  
603 close or connected to the land surface such that any fluctuation in groundwater table can result in considerable change  
604 in surface runoff [Werner and Simmons, 2009; Michael et al., 2013]. In the selected cross sections our study, the steeper  
605 one (slope 1:20) aquifer of C1 is a partially topography-limited system (e.g. Figure 75a, b) (the hillslope is recharge-  
606 limited while the valley bottom is topography-limited). ~~In C2~~ The flat one (slope 1:1000) the aquifer is transformed  
607 into a fully recharge-limited system (from Figure 75b ~~to 5e~~) due to the reduced hydraulic head gradients. This  
608 transformation leads to three main effects: (i) The seepage flow vanishes because the groundwater table disconnects  
609 from the land surface. The seepage route that would discharge water from the top of hillslope to the stream is cut off,  
610 This transformation switches off the preferential flow paths via seepage to the land surface and significantly reduces  
611 the  $YF_Q$ .

612 ~~Reducing the topographic slope to 1:60 does not significantly change the flow pattern (Figure 5b). However, the~~  
613 ~~spatially averaged depth of the groundwater table is reduced from 1.5 m to 0.8 m (Figure 4d). This change leads to~~  
614 ~~two main effects: (i) the infiltration processes is weakened, indicated by the fact that the portion of subsurface domain~~  
615 ~~characterized by vertical flow is reduced from 34% to 18.22%, and (ii) the shallow subsurface flow processes, such~~  
616 ~~as seepage, are promoted, increasing the amount of water taking the short shallow flow paths in the system. This is~~  
617 ~~proved by that the portion of streamflow generated by surface run-off increased from 3.2 m<sup>3</sup>/day to 7.1 m<sup>3</sup>/day (Figure~~  
618 ~~5a, b).~~

619  
620 ~~Subsequently, the contribution of young water to streamflow significantly increases when the slope decreases from~~  
621 ~~1:20 to 1:60, also supported by the computed TTDs (Figure 6a). Given that the groundwater storage significantly~~  
622 ~~increases with decreasing slope, this effect is similar to the “inverse storage effect” that has been described in Harman,~~  
623 ~~[2015] as the relative contribution of young water to stream flow increasing with increasing storage. Kim et al., [2016]~~  
624 ~~also reported based on their lysimeter experiments that younger water was discharged in greater proportion under~~  
625 ~~wetter conditions compared to drier conditions. However, the observed changes in groundwater table depth (thus~~  
626 ~~storage) in our study were caused by topography rather than by climate.~~

627 ~~(3) For C3 (slope 1:100 — 1:1000), the aquifer is fully recharge limited without any preferential flow via land surface.~~  
628 ~~Further reducing the topographic slope to 1:1000 mainly changes the spatial distribution of the unsaturated zone~~  
629 ~~(comparing Figure 5d with 5c). Because the groundwater table depth (thus the storage) more or less remains~~  
630 ~~unchanged (Figure 4d), interestingly, here the “inverse storage effect” does not apply anymore and cannot explain the~~  
631 ~~increase of the  $YF_Q$  when the topography becomes flatter.~~

632 ~~However, on flatter landscapes, local flow cells are more likely to form, where water infiltrates to the aquifer and~~  
633 ~~eventually exits the aquifer via ET rather than via flow to the stream (Figure 7.5b), the local flow cells are more~~  
634 ~~pronounced in the dry season, see Figure S31-b in the supporting information).~~

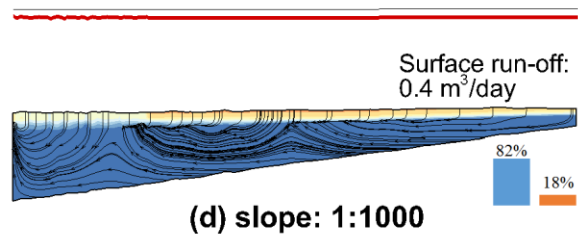
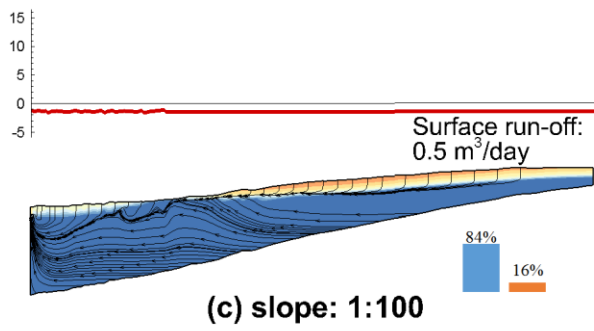
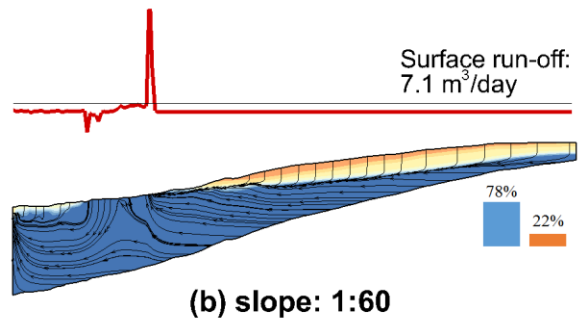
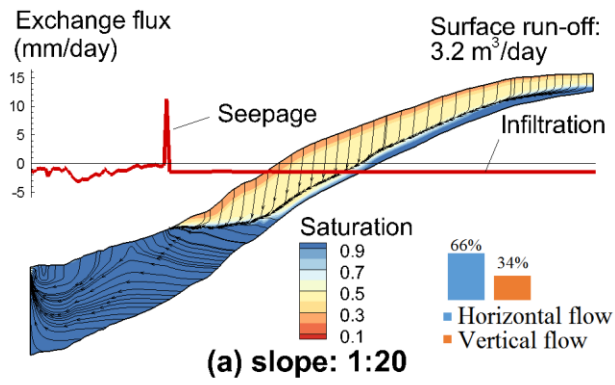
635 ~~Because of the three aforementioned three effects, simply put, the connectivity between the stream and the more distant~~  
636 ~~hillslopes is significantly reduced. Precipitation falling farther from the stream has a lower chance to reach the stream~~  
637 ~~and a higher chance to be intercepted by ET on its way to the stream, because the hillslope that used to generate~~  
638 ~~old streamflow does not contribute to streamflow anymore. flow velocity is much lower due to the smaller horizontal~~  
639 ~~component of hydraulic head gradient. While precipitation water close to the stream has a higher chance to contribute~~  
640 ~~to streamflow. We hypothesize concluded that the increase of the  $YF_Q$  in flat landscapes as indicated by the computed~~  
641 ~~TTDs (Figure 6b), is due to this reduction of the longer flow paths and the persistence of shorter flow paths, as~~  
642 ~~indicated by the computed TTDs (Figure 7c).~~

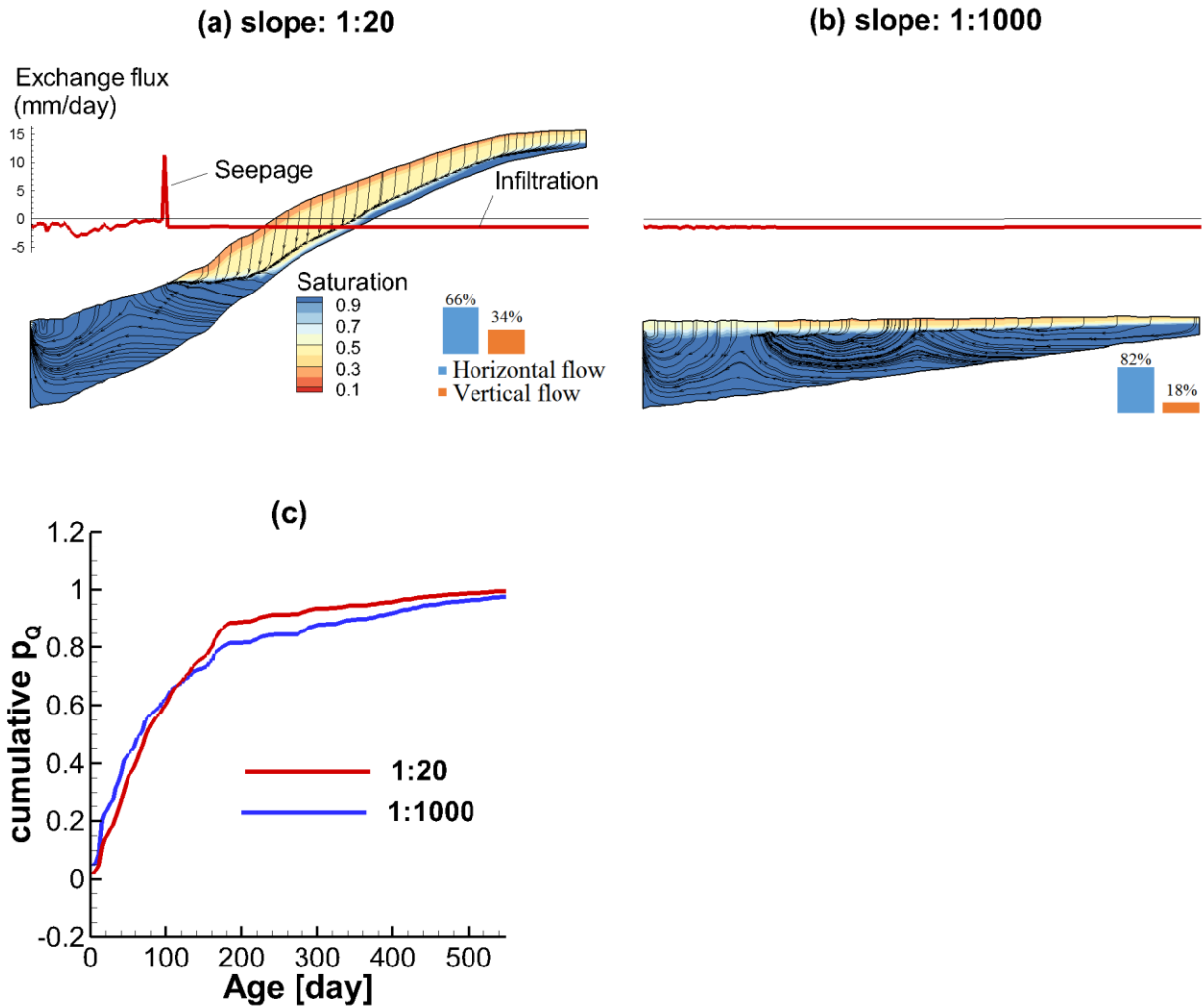
643 ~~To further verify our hypothesis, we mapped the land area contributing to the streamflow (streamflow generation zone)~~  
644 ~~using a particle tracking algorithm in HydroGeoSphere [Yang et al., 2018]. Figure 7 demonstrates the streamflow~~  
645 ~~generation zone in February for the slope 1:100 and 1:1000, respectively. For the aquifer with a slope of 1:100, the~~  
646 ~~zone extends further into the hillslope, with relatively younger streamflow generated close to the stream and old~~

647 ~~streamflow (i.e. age > 5 years) generated further up the hillslope. When the slope is reduced to 1:1000, the streamflow~~  
648 ~~generation zone is much closer to the stream. The hillslope that used to generate old streamflow does not contribute~~  
649 ~~to streamflow anymore. This means that in flatter landscapes, the evolution of local flow cells reduces the connectivity~~  
650 ~~between the stream and the more distant hillslopes by intercepting the longer flow paths at the land surface before~~  
651 ~~they can reach the stream (Figure 7b), leading to an increase in the  $YF_{\theta}$ . We refer to this as the “local flow cells effect”.~~

652

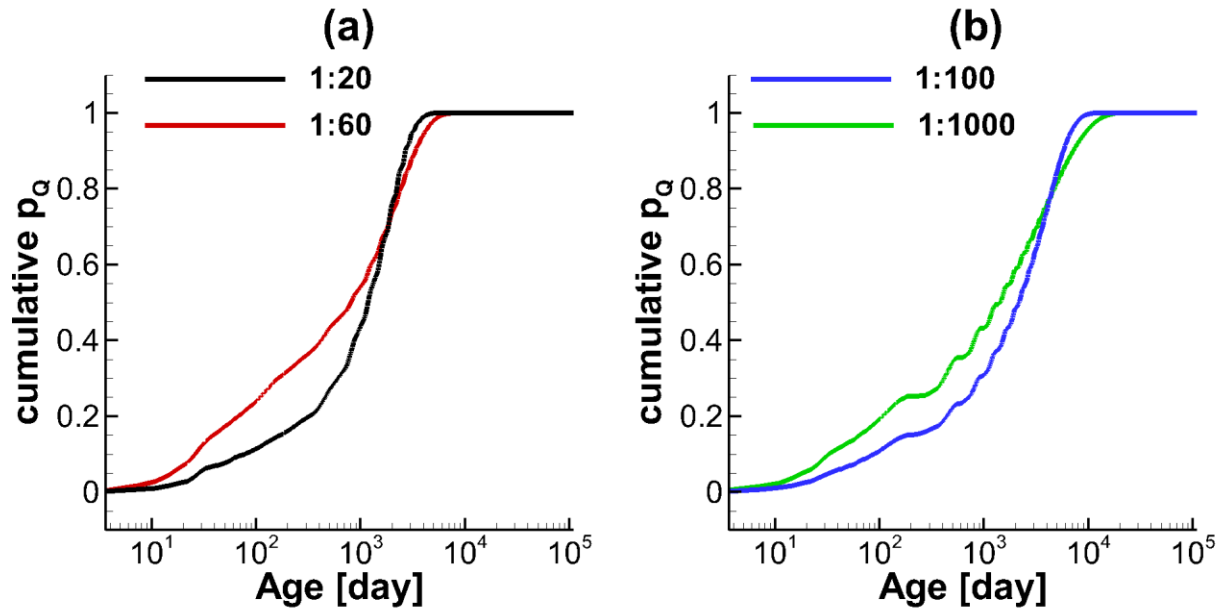
653





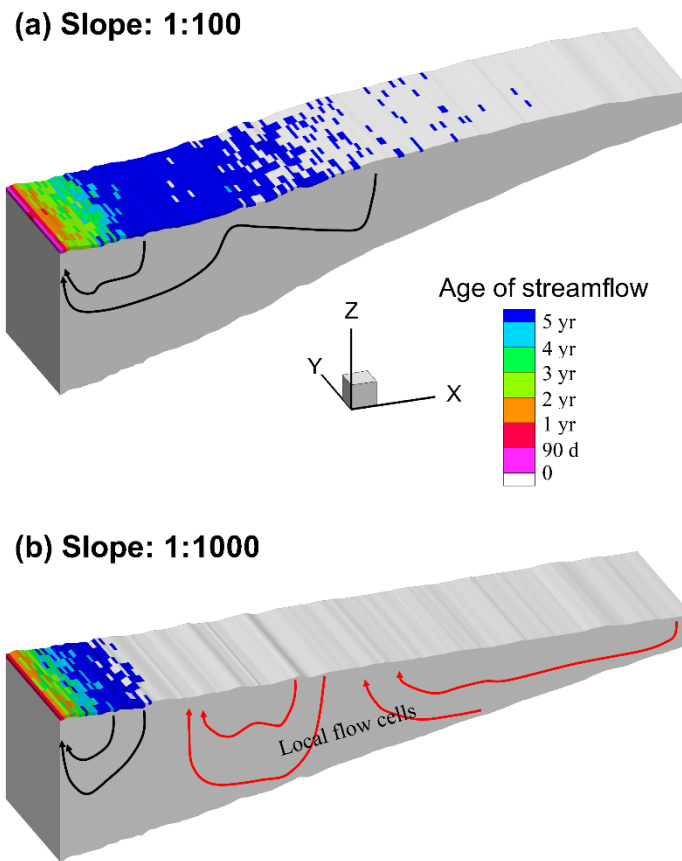
655  
 656 **Figure 75.** The cross-sectional view of the distributions of saturation, flow paths, and exchange fluxes between  
 657 the surface and the subsurface in the wet season (February) for the catchment aquifer with topographic slope (a)  
 658 1:20, and (b) 1:60, (c) 1:100, and (d) 1:1000. The cross-section is marked in Figure 1a. The black lines represent the  
 659 flow paths. The red curves show exchange fluxes (along the cross-sectional profiles), positive values indicate seepage  
 660 to the land surface and negative values indicate infiltration to the subsurface. (c) The computed cumulative TTDs for  
 661 Q during the wet season (February), for the catchment with topographic slope of 1:20 and 1:1000.





662  
 663  
 664  
 665  
 666

**Figure 6.** The computed cumulative TTDs for Q during the wet season (February), for the cross sections with topographic slope of (a) 1:20 and 1:60, and (b) 1:100 and 1:1000.



667 **Figure 7.** Maps showing the land areas that contribute to streamflow via subsurface flow through the aquifer with  
 668 topographic slopes of (a) 1:100 and (b) 1:1000. The color indicates the age of the streamflow. Black lines indicate the  
 669 flow paths to the stream, and red lines indicate the local flow cells that are not connected to stream.  
 670

671  
 672 In summary, we identified a generally increasing pattern of  $YF_o$  the young stream flow fraction in response to the  
 673 decreasing topographic slope. ~~three classes for the response of in stream concentrations to topographic slope under a~~  
 674 ~~humid climate.~~ When the landscape becomes flatter, the hydraulic head gradient as the main driving force, changes  
 675 the aquifer from a partially topography-limited system ~~with preferential overland flow (C1)~~ to a recharge-limited  
 676 system that is more likely to form local flow cells ~~(C3)~~. ~~For the aquifer of C2, which is a transitional class between~~  
 677 ~~C1 and C3,  $YF_o$  and nitrate concentrations experience a sharp drop once the preferential overland flow paths cannot~~  
 678 ~~be maintained.~~ For the aquifer of C1 (or C3), decreasing slopes tend to generate a higher fraction of young streamflow  
 679 and export nitrate at higher concentrations. However, the former is dominated by the “inverse storage effect” while  
 680 the latter is dominated by the “local flow cells effect”. In this sense, the response of in stream concentrations to  
 681 topographic slope is threshold-like rather than monotonous.

682

### 4.3 Effect of topographic slope on N export

Simulated results show that the topographic slope can influence the N loads and fluxes in the catchments. Figure 8a demonstrates that the SIN tends to be higher in flatter landscape and lower in steeper landscapes. This generally indicates that the flat landscape has a higher potential to retain the N in the soil. However, the DIN is not significantly influenced by the topographic slope. N fluxes of leaching and export to the stream exhibit the opposite pattern. For the N fluxes, the leaching into groundwater decreases with the decrease of topographic slope (Figure 8b). This is mainly because the flow velocity (influencing the leaching rate according to equation 6) in flatter landscape is lower due to the reduced hydraulic head gradient. Comparing the time-variable leaching between the steepest and flattest catchments (slope 1:20 and 1:1000, Figure 8c), it can be observed that the leaching reduction in the flatter landscape mainly occurs in the wetting period (Nov to Dec). This may be because that the responses of flow velocity in the flatter catchment is not as large as that in the steeper catchment when the system transitions from dry to wet conditions. A large portion of the leached N mass has been degraded during transport in the groundwater, with the fraction rising from 80% in the steepest landscape to 95% in the flattest landscape (Figure 8b). Mechanically, the reduced connectivity between the stream and more distant hillslopes in flatter landscapes inhibits the N export to the stream and promoting the degradation by increasing the N residence time in the catchment. Subsequently, the N export shows a decreasing pattern with the decrease of topographic slope (Figure 8b).

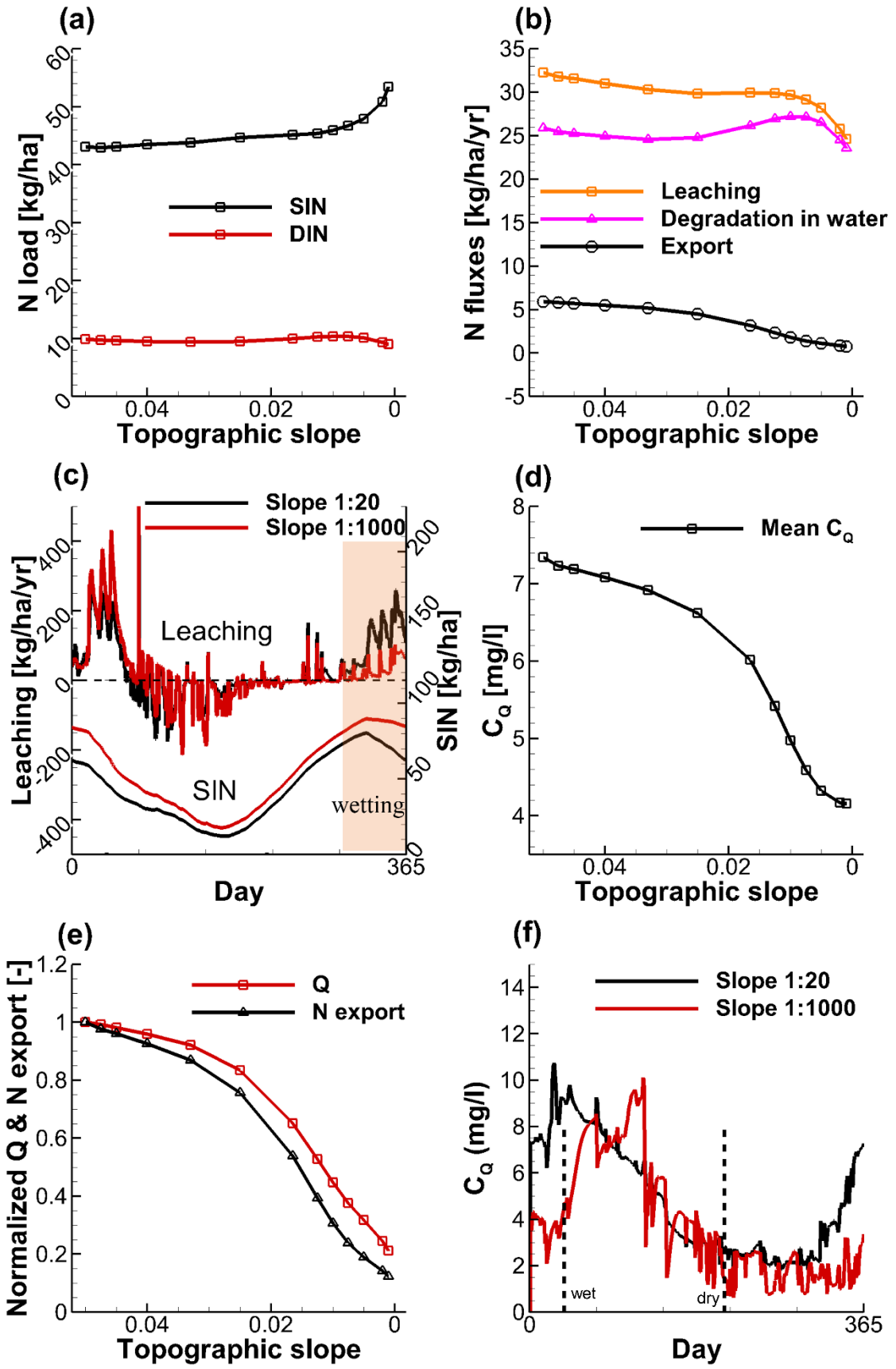
Figure 4a-The calculated flow-weighted shows that the mean  $C_Q$  shows a decreasing trend in response to the decreasing changes in topographic slope (Figure 8d): (1) the mean  $C_Q$  increases when the topographic slope decreases from 1:20 to 1:60, (2) the mean  $C_Q$  drops sharply when the topographic slope further decreases to 1:100, and (3) the mean  $C_Q$  increases again when the topographic slope decreases from 1:100 to 1:1000, from  $7.3 \text{ mg l}^{-1}$  in the steepest catchment and to  $4.2 \text{ mg l}^{-1}$  in the flattest catchment. Even though both of Q and N export show decreasing patterns with the decrease of topographic slope, the N export decreases to a higher degree than Q, indicated by their normalized values (Figure 8e). Comparing the time-variable  $C_Q$  between the steepest and flattest catchments (slope 1:20 and 1:1000, Figure 8f), it can be observed that the topographic slope influences the  $C_Q$  in two ways: (i) The  $C_Q$  is generally lower (but not always) in the flatter landscape over most of the time in a year, and (ii) the high peaks of  $C_Q$  in flatter landscapes are delayed in time. However, both of the high concentrations always occur in the wet periods (Jan – Apr) and low concentrations always occur in the dry periods (Jul – Oct). The maximum and minimum values are reached at topographic slopes of 1:60 and 1:100, respectively, rather than in the flattest or steepest landscapes. According to the distinct responses within different ranges of topographic slopes, we sorted the virtual catchments into three classes in terms of the mean topographic slopes of the aquifer (or the landscape) as follows (Figure 4a):

**C1**, with topographic slope in the range [1:20 — 1:60]

**C2**, with topographic slope in the range [1:60 — 1: 100]

**C3**, with topographic slope in the range [1: 100 — 1: 1000]

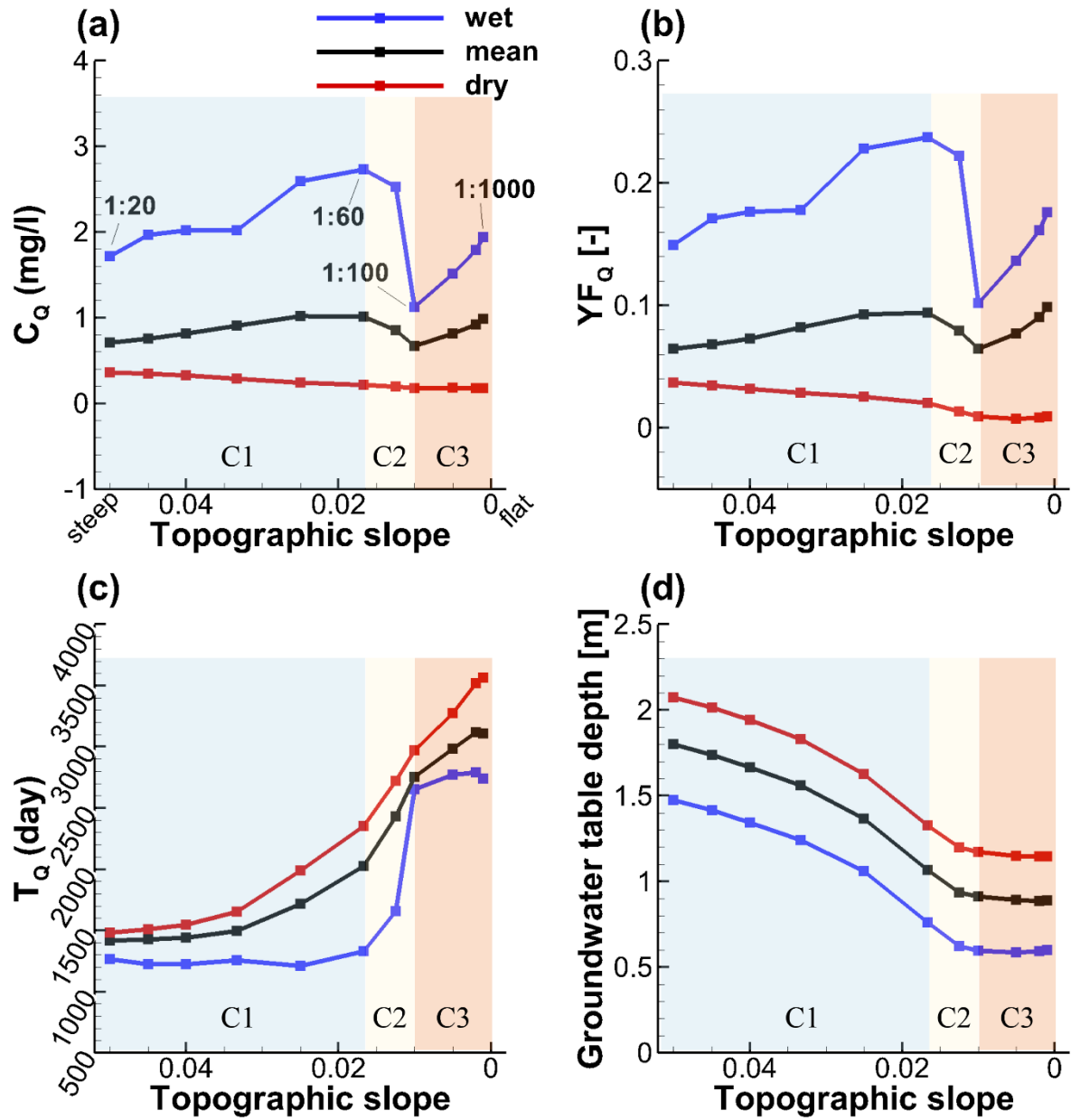




720 **Figure 8.** The simulated (a) N loads, (b) N fluxes in relation to the topographic slope for the simulated catchments.  
721 (c) Comparison of the time variable N loads and fluxes between a steep landscape (slope 1:20) and a flat landscape  
722 (slope 1:1000). The simulated (d) flow-weighted mean  $C_Q$ , and (e) the normalized Q and N export (normalized to their  
723 values of the base scenario) in relation to the topographic slope. (f) Comparison of the time variable  $C_Q$  between a  
724 steep landscape (slope 1:20) and a flat landscape (slope 1:1000). Note that for the leaching fluxes in (c), positive  
725 values are referred to as the N leaching from the soil to the groundwater, negative values are referred to as the  
726 precipitation of N from groundwater to the soil by the evapoconcentration effect. The vertical dashed lines indicate  
727 the time when the catchment reaches the wettest (left) and the driest (right) conditions.

728  
729 A similar three-class response can be observed for the wet-time  $C_Q$  (blue line in Figure 4a), it is even more pronounced  
730 than the one for the mean  $C_Q$ . The dry-time  $C_Q$  decreases linearly from steeper to flatter landscapes, not exhibiting  
731 specific classes. The effect of topographic slope on  $C_Q$  is hence dominated by the wet season response as most of the  
732 discharge was produced during the wet season. The response pattern of the  $YF_Q$  is highly identical to the  $C_Q$  response  
733 patterns, also showing a three-class response (Figure 4b). This indicates that the topographic slope influences the  $C_Q$   
734 levels via changing the young water fraction. Figure 4c demonstrates that the discharge age  $T_Q$  tends to be younger in  
735 steeper and older in flatter landscapes, especially during the dry season. This pattern did not show any correlation to  
736 the response of  $C_Q$ , thus suggesting that discharge age  $T_Q$  is not the most valuable predictor of  $C_Q$ .

737  
738 Subsequently, the contribution of young water to streamflow significantly increases when the slope decreases from  
739 1:20 to 1:60, also supported by the computed TTDs (Figure 6a). Given that the groundwater storage significantly  
740 increases with decreasing slope, this effect is similar to the “inverse storage effect” that has been described in Harman,  
741 [2015] as the relative contribution of young water to stream flow increasing with increasing storage. Kim et al., [2016]  
742 also reported based on their lysimeter experiments that younger water was discharged in greater proportion under  
743 wetter conditions compared to drier conditions. However, the observed changes in groundwater table depth (thus  
744 storage) in our study were caused by topography rather than by climate.



746  
 747  
 748 **Figure 4.** The simulated (a) in-stream concentration  $C_Q$ , (b) young-water fraction in streamflow  $YF_Q$ , (c) discharge  
 749 age  $T_Q$ , and (d) spatially averaged depth of the groundwater table from the land surface, in relation to the topographic  
 750 slope for the simulated cross-sections. The temporal mean, the dry time value and the wet time value of these variables  
 751 were plotted. C1, C2 and C3 represent the landscape classes 1, 2, and 3, respectively.

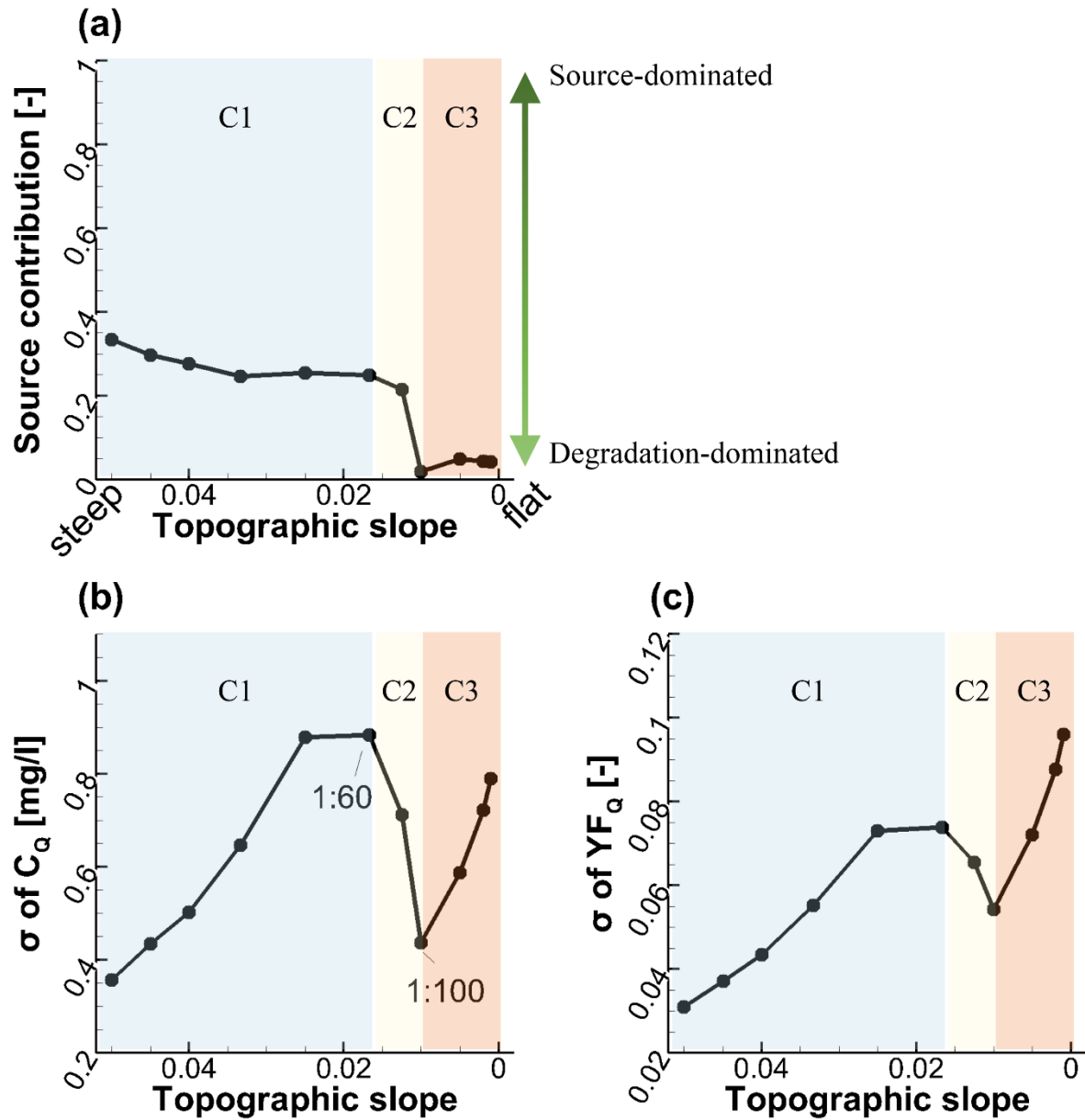
752 The response of the source contributions to topographic slope is threshold like (Figure 8a): the source contributions  
 753 in C1 were significantly higher than the ones in C3. Especially for the landscapes of C3, the fluctuation of  $C_Q$  was  
 754 hardly impacted by source variability. Mechanically, the seasonal source fluctuation is more likely to be damped by  
 755 relatively longer transit times in C3 landscapes, which are relatively flat.

756 Given that the seasonal  $C_D$  variation can be attributed more to the variation in transit times (thus to the variation in the  
757  $YF_D$ ), it was expected that the standard deviations of  $C_D$  and  $YF_D$  (Figure 8b, c) had similar responses to the topographic  
758 slope. Both of the responses exhibit a threshold-like pattern, similar to the response of the mean  $C_D$  (Figure 4a). This  
759 is because  $C_D$  during the dry season is generally low, regardless of whether the landscape is steeper or flatter. The  
760 overall response of  $\sigma(C_D)$  to topographic slope is determined by the response of the relatively high  $C_D$  during the wet  
761 season, and can be interpreted in the same three class pattern:  $\sigma(C_D)$  increases with the decrease of slope within C1  
762 (or C3), suggesting that flatter landscapes tend to export nitrate with more seasonal fluctuations in  $C_D$  for C1 (or C3).  
763 However, for C2, a significant drop in this fluctuation can be expected when the landscape transforms from C1 to C3.  
764 As a result, the maximum seasonal variation was reached at the slope of 1:60. For the mechanistic interpretation please  
765 refer to section 4.1.

766  
767

768





769  
770  
771

**Figure 8.** The calculated (a) source contribution to the variation of in-stream concentration  $C_Q$ , (b)  $\sigma$  of  $C_Q$ , (c)  $\sigma$  of  $YF_q$ . C1, C2 and C3 represent for the landscape classes 1, 2, and 3, respectively.

772

#### 773 4.4.3 Discussion

774 *Jasechko et al.*, [2016] reported that (the logarithm of) catchment topographic slope was significantly negatively  
775 correlated with young streamflow fractions with a spearman rank correlation of -0.36. This conclusion was made  
776 statistically based on their observed 254 sites. Our numerical study based on the eleven **cross-sectional**  
777 **aquifers/catchments** with different slopes but identical climate conditions resulted in more physically-based  
778 information that goes beyond such statistical correlations. Our results **confirms** show that young streamflow fraction

779 and slope ~~generally exhibit~~possess a ~~negative correlation~~threshold-like three-class relation instead of a monotonous  
780 relation. Additionally, our results show that the young water fraction in ET is positively correlated with the slope. The  
781 negative correlation between slope and young streamflow fraction can be found in slope classes C1 and C3, but not in  
782 the slope class C2.

783 ~~For~~From the steepest landscape to the flattest landscape, the landscapes of the C1 class, catchments are likely to  
784 transition from a ~~form a~~partially topography-limited flow system to a recharged limited system, with preferential flow  
785 paths due to ~~the~~the reduction of relatively high hydraulic gradient. The ~~g~~Groundwater table level storage is ~~more~~  
786 closer to the land surface~~larger~~, when the landscape becomes flatter. The ~~larger~~higher young streamflow fraction in  
787 flatter landscapes. The “inverse storage effect” explains the increases of young streamflow in flatter landscapes during  
788 the wet season. This is consistent with the statement made by Jasechko et al., [2016] ~~that~~as the young streamflow  
789 fraction is more prevalent in flatter catchments which are characterized by more shallow lateral flow and less vertical  
790 infiltration. This phenomenon is also consistent with a negative correlation between groundwater table depth and  
791 young streamflow fraction, which has been frequently reported [Bishop et al., 2004; Seibert et al., 2009; Frei et al.,  
792 2010; Jasechko et al., 2016]. Using the insight into the flow processes of the catchment, we found that the connectivity  
793 between the stream and the more distant hillslopes is reduced in flatter ~~For~~landscape, due to the ~~reduced~~vanished  
794 seepage flow, the weakened infiltration and the formation of local flow cells ~~that do not deliver flow~~reach to the  
795 stream. ~~of the C3 class, the negative correlation between young streamflow fraction and slope was also confirmed.~~  
796 However, here, the “inverse storage effect” fails to explain this correlation because neither the groundwater storage  
797 nor the groundwater table depth undergo any significant change. Our study points at out that the ~~the~~reduction of this  
798 connectivity, which results in the reduction of the longer flow paths and the persistence of shorter flow paths,  
799 formation of local flow cells that do not reach the stream ~~cause~~using the increase of ~~the~~ young streamflow fraction.

800 This phenomenon has not yet been reported to the best of our knowledge. However, for landscapes of the C2 class,  
801 our results suggest that young streamflow can be more prevalent in steeper landscapes with active preferential overland  
802 flow paths than in flatter landscapes with the fast preferential flow paths deactivated. This trend violates the otherwise  
803 negative correlation between topographic slope and young streamflow fraction. In this sense, the negative correlation  
804 between catchment topographic slope and young streamflow fraction is not conclusive.

805 Basically, the position of the groundwater table, flow path lengths and flow velocities, which are all different for  
806 different topographic slopes, jointly affect the young streamflow fractions ~~and nitrate export concentrations~~. Besides  
807 that, temporal variability of these three factors drives the distinct responses of the young streamflow fraction to  
808 topographic slope between seasons. ~~In our simulated catchments, the negative correlation between young streamflow~~  
809 ~~fraction and topographic slope is~~ For example, the three-class response is more pronounced in the ~~flat landscapes with~~  
810 ~~slopes < 1:60-wet winter than in the dry summer~~. This demonstrates that the system is complex and apparently contains  
811 various threshold effects disturbing a straightforward monotonous relationship between ~~any~~catchment characteristics  
812 (e.g. slope) and young water fraction (or streamflow concentration). In this sense, systematically investigating the  
813 reaction of the flow dynamics to catchment characteristic is necessary, rather than assuming a straightforward cause-  
814 effect relationship that can be misleading.

815

816 Our results demonstrate that stream water quality is potentially more-less vulnerable in flatter landscapes ~~when the~~  
817 ~~compared catchments have consistent flow patterns (e.g., both are C1 or C3 aquifers). The flatter landscapes tend to~~  
818 ~~retain/preserve~~ more N mass in the soil and export less N mass ~~into~~ the stream. ~~These~~ behaviors ~~can be~~ attributed  
819 ~~to (i) the reduced leaching in flat landscapes since~~as the decreased flow velocity physically reduces the potential of  
820 ~~water to solve and transport/wash~~ the solute, and (ii) the increased potential of degradation ~~because~~as the connectivity  
821 ~~between the stream and hillslope is blocked (i.e. there is more time for decay). The~~Our results also show that higher  
822  $C_0$  is more prevalent in steeper landscapes. Note that this is concluded ~~for in the perspective of average concentrations~~.  
823 Observations from the Selke catchment, central Germany shows that the  $C_0$  is not always lower in ~~the flatter lower~~  
824 regions [Dupas et al., 2017; Nguyen et al., 2022]. In the future mMore attention should be paid to the temporal  
825 variation and the time-scale concerning the effect of topographic slope on  $C_0$ . Additionally, our results show that we  
826 can expect lower  $C_0$  and higher young streamflow fractions in flatter landscapes ~~is where lower  $C_0$  and higher young~~  
827 streamflow fraction are expected. This ~~highlight~~ suggests ~~that~~, ~~concerning~~ with regard to the N transport in  
828 catchments, a large/high level of young streamflow fractions is not sufficient for high levels of  $C_0$ . This phenomenon  
829 has not yet been reported to the best of our knowledge. ~~e~~ importance of fast preferential flow on exporting the young  
830 water and nitrate. In mountainous central German catchments, these groundwater seepages to the land surface can be  
831 frequently observed. They can be identified as “hot spots” allowing for the export of nutrients with higher  
832 concentrations. This suggests that more attention should be paid to catchments with “hot spots” concerning the  
833 management of stream water quality and agricultural activity.

834 Concerning the seasonal variations of ~~nitrate export~~  $C_0$ , our results showed that significant seasonal variation can be  
835 expected under ~~such~~ temperate humid climates regardless of topographic slope. The high peak concentrations  
836 occurred in the wet and the low in the dry seasons, being consistent with the findings of previous studies [Benettin et  
837 al. 2015; Harman, 2015; Kim et al., 2016; Yang et al., 2018]. However, the topographic slope can slightly shift the  
838 high peak concentrations in time.

839 ~~The lowest concentrations were hardly affected by topographic slope, therefore the magnitude of seasonal variations~~  
840 ~~depended on how high the  $C_0$  rises during the wet seasons. This indicates that, for similar catchments in temperate~~  
841 ~~humid climates, a high mean in stream concentration level also means a high seasonal variation. The source~~  
842 ~~contribution to seasonal variations is higher for C1 landscapes ( $> 0.2$ ) than for C3 landscapes (almost zero). This~~  
843 ~~implies that changes in the nitrate source input due to, e.g., changing crop type, land use or fertilizer application~~  
844 ~~amount, are more likely to cause a detectable short term (e.g. seasonal) response of the in-stream concentration for~~  
845 ~~mountainous catchments. For flat landscapes, this response would be weaker.~~

846

#### 847 **4.54 Limitations and outlook**

848 The cross-comparison between ~~cross-sectional aquifers/catchments~~ with differing topographic slopes provides  
849 physically-based insights into the effects of topographic slope on nitrate export responses in terms of N fluxes and

850 mean concentrations ~~level and seasonal variations~~. However, this study is limited in scope in that it neglects other  
851 factors that may also have important impacts on the young streamflow and nitrate export processes:

852 First, ~~the our study only considered the modeled cross-sectional~~ aquifers ~~that is were~~ unconfined with an impermeable  
853 base and prescribed heterogeneity. ~~Our model conclusions may be limited to the regional scale~~. Other catchment  
854 characteristics such as landscape aspect, catchment area, aquifer permeability or drainage ability, aquifer depth, stream  
855 bed elevation, ~~and~~ fractured bedrock permeability, ~~bedrock slope and shape of basin~~ can potentially change the flow  
856 patterns and age composition in streamflow [McGlynn *et al.*, 2003; Broxton *et al.*, 2009; Sayama and McDonnell,  
857 2009; Stewart *et al.*, 2010; Jasechko *et al.*, 2016; Heidbüchel *et al.*, 2013, 2020; [Zarlenga and Fiori, 2020](#)]. For  
858 example, aquifers with high permeability or highly fractured bed rock are more likely to use deep rather than shallow  
859 flow paths and preferential discharge routes that lead to rapid drainage. Apart from that, it was reported that  
860 hydrological features such as precipitation variability, ET, antecedent soil moisture are also significantly linked to  
861 transit times [Sprenger *et al.*, 2016; Wilusz *et al.* 2017; Evaristo *et al.*, 2019; Heidbüchel *et al.*, 2013, 2020]. For  
862 example, compared to uniform precipitation, event-scale precipitation is more likely to trigger rapid surface runoff  
863 and intermediate flow, such that the contribution of young water from storage to streamflow can be increased.  
864 Therefore, further research should consider a more complex model structure involving various heterogeneity and  
865 climate types.

866 Second, several main simplifications were used in the formulation of [the](#) nitrate transport processes. (i) Transport  
867 modelling employed a constant degradation rate coefficient assuming that transit time was the only factor to determine  
868 degradation. This assumption neglected other factors that can spatially and temporally affect denitrification rates, such  
869 as temperature, redox boundaries (e.g., high oxygen concentration in shallow flow paths), [the](#) amount of other nutrients  
870 (e.g. carbon), which also contribute to the seasonality in nitrate concentrations [Böhlke *et al.*, 2007]. Apart from that,  
871 we did not account for the long-term (decades [Van Meter *et al.*, 2017]) nitrate legacy effect as the dissolved nitrate  
872 in groundwater reservoirs degraded continuously in our model, which would not occur in older reservoirs where the  
873 denitrification is very slow or deactivated (e.g. due to the lack of [a](#) carbon source). (ii) ~~In our simulations, the~~  
874 ~~complexities of the nitrogen pool were simplified by integrally defining a source concentration curve. The variability~~  
875 ~~of the source input was implicitly considered by forcing the source concentration to vary along that curve over the~~  
876 ~~course of a year. The accurate simulation of  $C_Q$  would depend on a realistic estimation of the input source curve.~~  
877 ~~However, it is not that important in our study as we were focused on understanding how the response changes with~~  
878 ~~regard to topographic slope rather than on accurately reproducing  $C_Q$ .~~ (iii) ~~The nitrate external input~~ source was  
879 uniformly applied across the land surface in our modelling. However, strong source heterogeneity may exist in  
880 catchments. For example, the ~~N external input source concentrations varies~~ between land uses or along the soil profile  
881 [Zhi *et al.*, 2019]. This spatial source heterogeneity could affect the seasonal variations of  $C_Q$  [Musolff *et al.*, 2017;  
882 Zhi *et al.*, 2019] and should be considered in further research.

883 Despite these limitations, the numerical experiments in this study could clearly identify ~~a three-class~~ [the](#) response of  
884 young streamflow and nitrate export to topographic slope under a humid seasonal climate, and show that hydraulic  
885 gradient is an important factor causing ~~the flow field~~ differences between the ~~classes~~ [catchments](#). This was achieved

886 by using the advantages of a physically-based flow simulation that allows for a more mechanistic evaluation of flow  
887 processes, which would be impossible with a purely data driven analysis based on, e.g., isotopic tracers only.

888

## 889 5 Conclusions

890 Previous data driven studies suggested that catchment topographic slope impacts the age composition of streamflow  
891 and consequently the in-stream concentrations of certain solutes [Jasechko *et al.*, 2016]. We attempted to find more  
892 mechanistic explanations for these effects. We chose ~~a cross-section from~~ the small agricultural catchment ‘Schäferfald’  
893 in Central Germany and, based on it, generated eleven synthetic ~~cross-sections~~catchments of varying topographic  
894 slope. The groundwater and overland flow, and the ~~nitrate-N~~ transport in these ~~cross-sections~~catchments were  
895 simulated using a coupled surface-subsurface model. Water age compositions for Q and ET were determined using  
896 numerical tracer experiments. Based on the calculated flow patterns, ~~in-stream nitrate concentration  $C_Q$  and~~ young  
897 water fractions in streamflow  ~~$YF_Q$ , N mass fluxes and in-stream nitrate concentration  $C_Q$~~ , we systematically assessed  
898 the effects of varying catchment topographic slopes on the nitrate export dynamics in terms of the mass fluxes and  
899 annual mean concentration levels ~~(annual mean) and its seasonal variability~~. The main conclusions of this study are:

- 900 • Under the considered humid climate,  ~~$YF_Q$ ,  $C_Q$~~  is generally negatively correlated ~~related~~ to topographic slope  
901 ~~by a three-class response~~. When the landscape becomes flatter, the hydraulic head gradient is the main driving  
902 force ~~to~~, change~~changing~~ the aquifer from a partially topography-limited system ~~with preferential overland~~  
903 ~~flow (C1)~~ to a recharge-limited system, reducing the connectivity between the stream and the more distant  
904 hillslopes that is more likely to form local flow cells (C3). This change results in the reduction of longer flow  
905 paths and the persistence of shorter flow paths, subsequently causing the ~~For landscapes falling into the~~  
906 ~~classes C1 or C3, flatter landscapes tend to generate more younger~~ streamflow and export nitrate of higher  
907  ~~$C_Q$~~ . However, for the former this is due to the “inverse storage effect” and for the latter this is due to the  
908 “local flow cells effect”. For the transitional class C2,  ~~$YF_Q$  and nitrate concentration decrease sharply once~~  
909 ~~the flatter landscapes are no longer able to maintain the fast preferential overland flow paths~~.
- 910 • The flatter landscapes tend to retain/preserve more N mass in soil and export less N mass to the stream. These  
911 patterns are attributed to (i) the reduced leaching in flat landscape as the decreased flow velocity physically  
912 reduces the potential of water to transport/wash the solute towards the stream, and (ii) the increased potential  
913 of degradation as the connectivity between the stream and hillslope is blocked and the solute stays inside the  
914 aquifer longer. ~~For catchments in temperate humid climates with considerable seasonality in wetness~~  
915 ~~conditions, the seasonal variation of  $C_Q$  is dominated by the variability in transit times and in turn degradation,~~  
916 ~~rather than by the variability in the nitrate source. Especially for the aquifer of the C3 class, significant~~  
917 ~~seasonal variation of  $C_Q$  can be generated even without any variability in the nitrate source.~~
- 918 • For the considered catchment, the annual mean  $C_Q$  shows a decreasing trend in response ~~s~~ to the decreasing  
919 topographic slope, because the N export decreases to a higher ~~more in~~ degree than Q. Flatter landscapes tend

to generate ~~larger~~<sup>higher</sup> young streamflow fractions (but lower  $C_Q$ ), suggesting that a ~~large~~<sup>high</sup> level of young streamflow fractions is not sufficient for a high level of  $C_Q$ .

- ~~The response of the seasonal variation of  $C_Q$  to topographic slope is similar to the one of the mean  $C_Q$ . For the landscapes of the C1 or C3 classes, seasonal variation tends to be more pronounced for flatter landscapes. However, for the C2 class, a significant decrease in this variation can be expected when fast preferential overland flow paths are switched off on flatter landscapes.~~

Overall, this study provides a mechanistic perspective on how catchment topographic slope affects young streamflow fraction and nitrate export patterns. The use of a fully-coupled flow and transport model extends the approach to investigate the effects of catchment characteristics beyond the frequently used tracer data-driven analysis. It can be used for similar studies of other catchment characteristics and for other solutes. The results of this study improved the understanding of the effects of certain catchment characteristics on nitrate export dynamics with ~~reveal~~ potential implications for the management of stream water quality and agricultural activity, in particular for catchments in temperate humid climates with pronounced seasonality. Given the limitations of this study, future work should be devoted to improve the degradation formulation, to investigate further catchment characteristics, as well as to consider various climate types.

## Notation

$t$	[T] time
$T$	[T] age / transit time / residence time
$J$	[ $LT^{-1}$ ] precipitation
$ET$	[ $LT^{-1}$ ] evapotranspiration
$Q$	[ $LT^{-1}$ ] discharge / streamflow
$ps$	[-] age distribution of storage
$p_{ET/Q}$	[-] age distribution for evapotranspiration / discharge, equivalent to TTD
$C$	[ $ML^{-3}$ ] concentration
<del><math>C_j</math></del>	<del>[<math>ML^{-3}</math>] source concentration</del>
$C_Q$	[ $ML^{-3}$ ] in-stream solute (nitrate) concentration
$T_Q$	[ $ML^{-3}$ ] age (transit time) of discharge
<del><math>Da</math></del>	<del>[-] Damköhler number</del>
$YF_Q$	[-] young water fraction in streamflow, or young streamflow fraction
$YF_{ET}$	[-] young water fraction in ET
<u><math>SON</math></u>	<u>[<math>ML^{-2}</math>] soil organic nitrogen</u>
<u><math>SIN</math></u>	<u>[<math>ML^{-2}</math>] soil inorganic nitrogen</u>
<u><math>DIN</math></u>	<u>[<math>ML^{-2}</math>] dissolved inorganic nitrogen in water</u>

956

957

958 **Code/Data availability**

959 All data used in this study are listed in the supporting information and uploaded separately to HydroShare [Yang,  
960 2022~~9~~].

961

962 **Author contributions**

963 JY: conceptualization, methodology, software, formal analysis, visualization, writing - review & editing; **QW**:  
964 modelling, analysis, writing; IH: writing - review & editing; CL: conceptualization, methodology, review & editing;  
965 YX: methodology; AM: conceptualization; JF: conceptualization, review & editing.

966

967 **Competing interests**

968 The authors declare that they have no conflict of interest.

969

970 **Acknowledgments**

971 This research was supported by the National Natural Science Foundation of China (No. 52009032), and the  
972 Fundamental Research Funds for the Central Universities (No. B210202019).

973

974 **References**

975 Anis, M. R., & Rode, M. (2015). Effect of climate change on overland flow generation: A case study in central  
976 Germany. *Hydrological Processes*, 29(11), 2478–2490.

977 Benettin, P., Y. van der Velde, S. E. A. T. M. van der Zee, A. Rinaldo, and G. Botter (2013), Chloride circulation in  
978 a lowland catchment and the formulation of transport by travel time distributions, *Water Resources Research*, 49(8),  
979 4619–4632, doi: 10.1002/wrcr.20309.

980 Benettin, P., J. W. Kirchner, A. Rinaldo, and G. Botter (2015), Modeling chloride transport using travel time  
981 distributions at plynlimon, wales, *Water Resources Research*, 51(5), 3259–3276, doi:10.1002/2014WR016600.

982 Bishop, K., Seibert, J., Köhler, S. and Laudon, H. (2004), Resolving the Double Paradox of rapidly mobilized old  
983 water with highly variable responses in runoff chemistry. *Hydrol. Process.*, 18: 185-189.  
984 <https://doi.org/10.1002/hyp.5209>.

985 [Botter, G., Bertuzzo, E., & Rinaldo, A. \(2010\). Transport in the hydrologic response: Travel time distributions, soil  
986 moisture dynamics, & the old water paradox. \*Water Resources Research\*, 46\(3\).  
987 <https://doi.org/10.1029/2009WR008371>.](#)

988 [Botter, G., Bertuzzo, E., & Rinaldo, A. \(2011\). Catchment residence and travel time distributions: The master  
989 equation. \*Geophysical Research Letters\*, 38\(11\). <https://doi.org/10.1029/2011GL047666>.](#)



990 Böhlke, J. K., M. E O'Connell, and K. L Prestegard (2007), Ground water stratification and delivery of nitrate to an  
991 incised stream under varying flow conditions, *Journal of environmental quality*, 36, 664–80,  
992 doi:10.2134/jeq2006.0084.

993 Broxton, P. D., P. A. Troch, and S. W. Lyon (2009), On the role of aspect to quantify water transit times in small  
994 mountainous catchments, *Water Resour. Res.*, 45, W08427, doi:10.1029/2008WR007438.

995 [Doherty, J., Hunt, R., 2010. Approaches to highly parameterized inversion – a guide to using PEST for groundwater-](#)  
996 [model calibration. Technical Report, USGS Survey Scientific Investigations Report. 2010-5169.](#)

997 Dupas, R., A. Musolff, J. W. Jawitz, P. S. C. Rao, C. G. Jäger, J. H. Fleckenstein, M. Rode, and D. Borchardt (2017),  
998 Carbon and nutrient export regimes from headwater catchments to downstream reaches, *Biogeosciences*, 14(18),  
999 4391–4407, doi:10.5194/bg-14-4391-2017.

1000 Evaristo, J., Kim, M., van Haren, J., Pangle, L. A., Harman, C. J., Troch, P. A., & McDonnell, J. J. (2019).  
1001 Characterizing the fluxes and age distribution of soil water, plant water, and deep percolation in a model tropical  
1002 ecosystem. *Water Resources Research*, 55(4), 3307-3327.

1003 Frei, S., Lischeid, G. and Fleckenstein J.H. (2010) Effects of micro-topography on surface-subsurface exchange and  
1004 runoff generation in a virtual riparian wetland – a modeling study, *Advances in Water Resources*, 33(11):1388-1401.

1005 [Haag, D., Kaupenjohann, M., 2001. Landscape fate of nitrate fluxes and emissions in central Europe: a critical review](#)  
1006 [of concepts, data, and models for transport and retention. \*Agric. Ecosyst. Environ.\* 86 \(1\), 1–21.](#)

1007 Harman, C. J. (2015), Time-variable transit time distributions and transport: Theory and application to storage-  
1008 dependent transport of chloride in a watershed, *Water Resources Research*, 51(1), 1–30, doi:10.1002/2014WR015707.

1009 Harman, C. J. (2019). Age-Ranked Storage-Discharge Relations: A Unified Description of Spatially Lumped Flow  
1010 and Water Age in Hydrologic Systems. *Water Resources Research*, 55(8), 7143-7165.

1011 Heidbüchel, I., P. A. Troch, and S. W. Lyon (2013). Separating physical and meteorological controls of variable transit  
1012 times in zero-order catchments. *Water Resources Research*, 49, 7644–7657, doi:10.1002/2012WR013149.

1013 Heidbüchel, I., J. Yang, A. Musolff, P. Troch, T. Ferré J. H. Fleckenstein (2020). On the shape of forward transit time  
1014 distributions in low-order catchments. *Hydrology and Earth System Sciences*, doi: 10.5194/hess-2019-440.

1015 Hrachowitz, M., O. Fovet, L. Ruiz, and H. H. G. Savenije (2015), Transit time distributions, legacy contamination  
1016 and variability in biogeochemical 1/f scaling: how are hydrological response dynamics linked to water quality at the  
1017 catchment scale?, *Hydrological Processes*, 29(25), 5241–5256, doi:10.1002/hyp.10546.

1018 [Heumann, S., Ringe, H., Böttcher, J., 2011. Field-specific simulations of net N mineralization based on digitally](#)  
1019 [available soil and weather data. I. Temperature and soil water dependency of the rate coefficients. \*Nutr. Cycl.\*](#)  
1020 [Agroecosyst. 91 \(2\), 219–234. <https://doi.org/10.1007/s10705-011-9457-x>.](#)

1021 [Hofstra, N., Bouwman, A.F., 2005. Denitrification in agricultural soils: summarizing published data and estimating](#)  
1022 [global annual rates. \*Nutr. Cycl. Agroecosyst.\* 72 \(3\), 267–278. <https://doi.org/10.1007/s10705-005-3109-y>.](#)

1023 Hrachowitz, M., P. Benettin, B. M. Van Breukelen, O. Fovet, N. J. Howden, L. Ruiz, Y. Van Der Velde, and A. J.  
1024 Wade (2016), Transit times-the link between hydrology and water quality at the catchment scale, *Wiley*  
1025 *Interdisciplinary Reviews: Water*, 3(5), 629–657.



1026 Jasechko, S., Kirchner, J., Welker, J. et al. Substantial proportion of global streamflow less than three months old.  
1027 Nature Geosci 9, 126–129 (2016). <https://doi.org/10.1038/ngeo2636>

1028 Kaandorp, V. P., Louw, P. G. B., Velde, Y., & Broers, H. P. (-2018). Transient Groundwater Travel Time Distributions  
1029 and Age - Ranked Storage - Discharge Relationships of Three Lowland Catchments. Water Resources Research, 54,  
1030 4519– 4536. <https://doi.org/10.1029/2017WR022461>

1031 Kim, M., L. A. Pangle, C. Cardoso, M. Lora, T. H. Volkmann, Y. Wang, C. J. Harman, and P. A. Troch (2016), Transit  
1032 time distributions and storage selection functions in a sloping soil lysimeter with time-varying flow paths: Direct  
1033 observation of internal and external transport variability, Water Resources Research, 52(9), 7105–7129.

1034 Li, Y., Chen, Y., Li, Z., 2019. Dry/wet pattern changes in global dryland areas over the past six decades. Glob. Planet.  
1035 Chang. 178, 184–192. <https://doi.org/10.1016/j.gloplacha.2019.04.017>.

1036 [Lindström, G., C.P. Pers, R. Rosberg, J. Strömqvist, and B. Arheimer \(2010\): Development and test of the HYPE](#)  
1037 [\(Hydrological Predictions for the Environment\) model – A water quality model for different spatial scales, Hydrol.](#)  
1038 [Res., 41.3–4, 295–319, 2010.](#)

1039

1040 McGlynn, B., J. McDonnell, M. Stewart, and J. Seibert (2003), On the relationships between catchment scale and  
1041 streamwater mean residence time, Hydrol. Processes, 17, 175– 181, doi:10.1002/hyp.5085.

1042 Michael, H.A., Russoniello, C.J., Byron, L.A., 2013. Global assessment of vulnerability to sea-level rise in  
1043 topography-limited and recharge-limited coastal groundwater systems. Water Resour. Res. 49, 1–13.

1044 Musolff, A., C. Schmidt, B. Selle, and J. H. Fleckenstein (2015), Catchment controls on solute export, Advances in  
1045 Water Resources, 86, 133–146.

1046 Musolff, A., J. H. Fleckenstein, P. S. C. Rao, and J. W. Jawitz (2017), Emergent archetype patterns of coupled  
1047 hydrologic and biogeochemical responses in catchments, Geophysical Research Letters, 44(9), 4143–4151,  
1048 doi:10.1002/2017GL072630.

1049 Nguyen, T. V., Kumar, R., Lutz, S. R., Musolff, A., Yang, J., & Fleckenstein, J. H. (2021). Modeling nitrate export  
1050 from a mesoscale catchment using storage selection functions. Water Resources Research, 57, e2020WR028490.  
1051 <https://doi.org/10.1029/2020WR028490>

1052 [Nguyen, T. V., Kumar, R., Musolff, A., Lutz, S. R., Sarrazin, F., Attinger, S., & Fleckenstein, J. H. \(2022\). Disparate](#)  
1053 [seasonal nitrate export from nested heterogeneous subcatchments revealed with StorAge Selection functions. Water](#)  
1054 [Resources Research, 58, e2021WR030797. https://doi.org/10.1029/2021WR030797](#)

1055 Oldham, C. E., D. E. Farrow, and S. Peiffer (2013), A generalized damköhler number for classifying material  
1056 processing in hydrological systems, Hydrology and Earth System Sciences, 17(3), 1133–1148, doi:10.5194/hess-17-  
1057 1133-2013.

1058 [Pierce, F. J., Shaffer, M. J., Halvorson, A. D. 1991. Chapter 12: Screening procedure for estimating potentially](#)  
1059 [leachable nitrate-nitrogen below the root zone. Managing Nitrogen for groundwater Quality and Farm Profitability,](#)  
1060 [Soil Science Society of America, USA, pp.259-283](#)

1061 Rinaldo, A., P. Benettin, C. J. Harman, M. Hrachowitz, K. J. McGuire, Y. Van Der Velde, E. Bertuzzo, and G. Botter  
1062 (2015), Storage selection functions: A coherent framework for quantifying how catchments store and release water  
1063 and solutes, *Water Resources Research*, 51(6), 4840–4847.

1064 Rodriguez, N. B., McGuire, K. J., & Klaus, J. (2018), Time-varying storage-water age relationships in a catchment  
1065 with a mediterranean climate. *Water Resources Research*, 54(6), 3988-4008.

1066 Sayama, T. & McDonnell, J. J. (2009), A new time-space accounting scheme to predict stream water residence time  
1067 and hydrograph source components at the watershed scale. *Wat. Resour. Res.* 45, W07401.

1068 Seibert, J., Grabs, T., Köhler, S., Laudon, H., Winterdahl, M., and Bishop, K.: Linking soil- and stream-water  
1069 chemistry based on a Riparian Flow-Concentration Integration Model, *Hydrol. Earth Syst. Sci.*, 13, 2287–2297,  
1070 <https://doi.org/10.5194/hess-13-2287-2009>, 2009.

1071 Sprenger, M., Seeger, S., Blume, T., & Weiler, M. (2016), Travel times in the vadose zone: Variability in space and  
1072 time. *Water Resources Research*, 52, 5727-5754.

1073 Therrien, R., McLaren, Sudicky, R. E., & Panday, S. (2010). *Hydrogeosphere: A three-dimensional numerical model*  
1074 describing fully-integrated subsurface and surface flow and solute transport, Groundwater Simulations Group.  
1075 Waterloo, ON: University of Waterloo.

1076 [Shaffer, M. J., Halvorson, A. D., Pierce, F. J. 1991. Chapter 13: Nitrate leaching and economic analysis package](#)  
1077 [NLEAP: model description and application. Managing Nitrogen for groundwater Quality and Farm Profitability, Soil](#)  
1078 [Science Society of America, USA. pp.285-322](#)

1079 Stewart, M. K., Morgenstern, U. & McDonnell, J. J. (2010), Truncation of stream residence time: how the use of stable  
1080 isotopes has skewed our concept of streamwater age and origin. *Hydrol. Process.* 24, 1646-1659.

1081 van der Velde, Y., G. De Rooij, J. Rozemeijer, F. Van Geer, and H. Broers (2010), Nitrate response of a lowland  
1082 catchment: On the relation between stream concentration and travel time distribution dynamics, *Water Resources*  
1083 *Research*, 46(11).

1084 [Stevenson, F.J., 1995. Humus chemistry: genesis, composition, reactions, Second Edition, Wiley. J Chem Educ. doi:](#)  
1085 [10.1021/ed072pA93.6, ISBN: 978-0-471-59474-1, 512 pp.](#)

1086 van der Velde, Y., P. J. J. F. Torfs, S. E. A. T. M. van der Zee, and R. Uijlenhoet (2012), Quantifying catchment-scale  
1087 mixing and its effect on time-varying travel time distributions, *Water Resources Research*, 48(6), n/a–n/a,  
1088 doi:10.1029/2011WR011310, w06536.

1089 Van Meter, K. J., N. B. Basu, and P. Van Cappellen (2017), Two centuries of nitrogen dynamics: Legacy sources and  
1090 sinks in the mississippi and susquehanna river basins, *Global Biogeochemical Cycles*, 31(1), 2–23,  
1091 doi:10.1002/2016GB005498.

1092 Werner, A. D., and C. T. Simmons (2009), Impact of sea-level rise on seawater intrusion in coastal aquifers, *Ground*  
1093 *Water*, 47, 197-204.

1094 Wilusz, D. C., Harman, C. J., & Ball, W. P. (2017). Sensitivity of catchment transit times to rainfall variability under  
1095 present and future climates. *Water Resources Research*, 53(12), 10231-10256.

1096 [Wijayantiati, Y., Budihardjo, K., Sakamoto Y., Setyandito, O. \(2017\). Topsoil N-budget model in orchard farming to](#)  
1097 [evaluate groundwater nitrate contamination. IOP Conf. Series: Earth and Environmental Science 109 \(2017\) 012034.](#)  
1098 [doi:10.1088/1755-1315/109/1/012034.](#)

1099 Yang, J., I. Heidbüchel, A. Musolff, F. Reinstorf, and J. H. Fleckenstein (2018), Exploring the dynamics of transit  
1100 times and subsurface mixing in a small agricultural catchment, *Water Resources Research*, 54(3), 2317–2335,  
1101 doi:10.1002/2017WR021896.

1102 [Yang, J., Heidbüchel, I., Musolff, A., Xie, Y., Lu, C.\\*, Fleckenstein, J.H. \(2021\). Using nitrate as a tracer to constrain](#)  
1103 [age selection preferences in catchments with strong seasonality, \*Journal of Hydrology\*, 603, 126889. doi:](#)  
1104 [https://doi.org/10.1016/j.jhydrol.2021.126889.](https://doi.org/10.1016/j.jhydrol.2021.126889)

1105 Yang, J. (2022). DS2022-12YJ, HydroShare,  
1106 <http://www.hydroshare.org/resource/e266298e55834617a26242f6af9687e1>

1107 [Zarlenga, A., & Fiori, A. \(2020\). Physically based modelling of water age at the hillslope scale: The Boussinesq age](#)  
1108 [equations. \*HYDROLOGICAL PROCESSES\*, 34\(12\), 2694-2706.](#)

1109

1110 [Zarlenga, A., Fiori, A., & Cvetkovic, V. \(2022\). On the interplay between hillslope and drainage network flow](#)  
1111 [dynamics in the catchment travel time distribution. \*HYDROLOGICAL PROCESSES\*, 36\(3\) \[10.1002/hyp.14530\].](#)

1112 Zhi, W., L. Li, W. Dong, W. Brown, J. Kaye, C. Steefel, and K. H. Williams (2019), Distinct source water chemistry  
1113 shapes contrasting concentration-discharge patterns, *Water Resources Research*, 55(5), 4233–4251,  
1114 doi:10.1029/2018WR024257.